



Transition path properties for one-dimensional systems driven by Poisson white noise



Hua Li^a, Yong Xu^{a,b,*}, Ralf Metzler^c, Jürgen Kurths^{d,e}

^a Department of Applied Mathematics, Northwestern Polytechnical University, Xi'an, 710072, China

^b MIIT Key Laboratory of Dynamics and Control of Complex Systems, Northwestern Polytechnical University, Xi'an, 710072, China

^c Institute for Physics & Astronomy, University of Potsdam, Potsdam-Golm 14476, Germany

^d Department of Physics, Humboldt University Berlin, Berlin, 12489, Germany

^e Potsdam Institute for Climate Impact Research, Potsdam 14412, Germany

ARTICLE INFO

Article history:

Received 30 June 2020

Revised 20 August 2020

Accepted 11 September 2020

ABSTRACT

We present an analytically tractable scheme to solve the mean transition path shape and mean transition path time of one-dimensional stochastic systems driven by Poisson white noise. We obtain the Fokker-Planck operator satisfied by the mean transition path shape. Based on the non-Gaussian property of Poisson white noise, a perturbation technique is introduced to solve the associated Fokker-Planck equation. Moreover, the mean transition path time is derived from the mean transition path shape. We illustrate our approximative theoretical approach with the three paradigmatic potential functions: linear, harmonic ramp, and inverted parabolic potential. Finally, the Forward Fluxing Sampling scheme is applied to numerically verify our approximate theoretical results. We quantify how the Poisson white noise parameters and the potential function affect the symmetry of the mean transition path shape and the mean transition path time.

© 2020 Elsevier Ltd. All rights reserved.

1. Introduction

The concept of first-passage times dates back to the investigation of financial market dynamics by Bachelier [1,2] and in the context of molecular chemical reactions by Smoluchowski [3]. The motivation was to pinpoint the time when a fluctuating stock price first crosses a given threshold or when a diffusing molecule first hits its reaction target. Today, first-passage theory is well established [4–6], albeit several breakthroughs have been reported within the last years. These include fundamental results for the (global) mean first-passage time in quite general settings [7–10] as well as the determination of the full distribution of first-passage times in generic geometries [11,12] as well as in potential landscapes [13–16]. The need for such refinements of first-passage theories comes from new experimental insight, for instance, finding that the geometric distance can indeed become relevant even in the confines of micron-sized bacteria cells [17–20]. In the context of molecular reactions or "narrow escape" through a small window in a bounded domain it is important to include the "reaction

limitation" in terms of a reaction barrier or an entropic constraint [21–25].

The crossing of an activation barrier in molecular reactions is at the heart of the famed Arrhenius law according to which the rate of a reaction is proportional to the Boltzmann factor for the "activation energy" E_a , i.e., the rate obeys $k \propto \exp(-E_a/k_B T)$ [26,27]. In most cases the barrier height $|E_a|$ considerably exceeds thermal energy $k_B T$ and the barrier crossing is thus a rare event. An important step in reaction rate theory was the formulation of transition state theory. We mention the two complementary pioneering approaches of Eyring [28] ("thermodynamic approach" [29]) and Wigner [30] ("classical mechanics approach" [31]). A kinetic pathway to rate laws was formulated by Kramers in his seminal work relating rate theory with the theory of Brownian motion [32]. For details we refer the readers to the authoritative review article by Hänggi, Talkner, and Borkovec [33].

Due to the large barrier height compared to thermal energy the system spends most of its time vibrating in a locally stable state, and the actual transition is a rare event. Experimentally, new experimental techniques such as single molecule spectroscopy allow unprecedented insights into individual transition paths of specific molecular reactions [34–38]. Single-molecule force spectroscopy, similarly, resolves transition path kinetics [39–41,58,59]. Simulations of transition paths relying on a naive simulation of

* Corresponding author at: Department of Applied Mathematics 127W Youyi Road, Xi'an 710072, China.

E-mail address: hsux3@nwpu.edu.cn (Y. Xu).

the process cannot generate sufficient statistics for such rare transition events within reasonable computing times. New sampling methods, based on original work by Chandler and coworkers [42,43] have become standard tools in reaction rate calculations [44–47].

Instead of considering all barrier crossing attempts, i.e., unsuccessful and successful ones, transition path theory focuses on "direct paths", i.e., those paths that successfully take the particle from its original point to the final point across the barrier. Somewhat counter-intuitively at first, there exists a time reversal symmetry between the successful barrier crossing path and the inverse path [43,46,47], and this equivalence even holds for the full distributions of crossing times [66]. The statistical properties of transition paths are thus vital for chemical reactions [33] and are extensively studied in modern transition state theory [63]. As transition paths resolve the transition time during direct crossing events they are of fundamental difference from the first-passage paths which could be obtained after implementing reflecting and absorbing boundaries for the transition region, as first-passage paths include all those "indirect" events, that repeatedly take the system back to its original state [51].

Mathematically, the transition paths are derived via installing two absorbing boundaries at the extreme points of transition region [52]. Some appropriate measures to quantify the transition paths are the transition path time (TPT) [53] and the transition path shape (TPS) [54]. The TPT plays an important role in transition paths and is conventionally defined as the time spent during direct transition paths. Generally, the TPT is a conditional first passage time (FPT) [41] of the switch events. The concept of the TPT is ubiquitously used in protein folding [55] and nucleic acid dynamics [37], pore transversal [56], ion channel crossing and polymer translocation [57]. In addition to the TPT, the TPS is a more detailed description of the transition path sequence as detailed below. Measuring the TPS thus provides a crucial characterization of the transition paths, and much effort has recently been dedicated to the development and analysis of transition paths with respect to both theoretical and experimental aspects.

The theoretical description of the transition path properties is often derived from the Fokker-Planck equation [60]. Many theoretical aspects of the transition path properties have been unveiled for the cases of a cusp barrier [61], conical tubes [62], or a parabolic potential [64] for overdamped and inertia-controlled cases [65]. Such simple potentials in which the transitions are driven by Gaussian white noise have been quite well studied. As mentioned, the mean TPT is identical in both directions for the case of Gaussian white noise [66], independent of any asymmetry in the potential. This symmetry, however, is broken in out of equilibrium situations with fluctuating forces [67]. The symmetry of the TPS [68] is affected by the potential function.

Here we demonstrate that the transition path dynamics changes dramatically in the presence of an alternative standard noise source, namely, Poisson white noise. In fact non-Gaussian white noise [69,70] has been observed in the fields of science, engineering, finance, and so on. Examples include the impact of traffic loads on road bridges and the excitation of ground structures by earthquakes [71], the Lotka-Volterra model [72], power grids [73], and damage evolution in mechanical systems due to wind or earthquakes [74]. It is essential to recognize that Poisson noise driven random processes are discontinuous, and the time and intensity of excitation are random. Recently, Poisson white noise [74] is getting popular since it provides a mathematical model to describe this kind of discontinuous random process, in contrast to Gaussian white noise [75]. Poisson white noise has been used with great success in the modeling of a series of independent and identically distributed random pulses, and the number of pulse arrival can be expressed by a Poisson counting process. Changes due to Poisson

white noise-driven jump processes include escape behavior [76], stationary response properties [77], non-stationary response behavior [78], extreme value distribution [79], and more. Here we aim at studying the effect of Poisson white noise on the transition path properties, based on a generalization of the theoretical description of transition paths. The challenge lies in the fact that there are infinite terms in the operator equations of the mean TPS and the mean TPT.

The central theme of this paper is to propose a new approximate theoretical approach to solve the mean TPS and the mean TPT of one-dimensional system driven by Poisson white noise. After truncating the equations satisfied by the mean TPS and the mean TPT, using a well-defined perturbation method, allows us to express the theoretical form of the mean TPS and the mean TPT. To demonstrate the generality of the proposed approximation approach, we apply the method to three types of simple potential functions: a linear potential, a harmonic ramp, and an inverted parabolic potential function. These three kinds of simple potential functions (see Fig. 1) are also the basis for the application to real systems, such as, the Malthusian model [80], the logistic map [81], and a micrometre-sized dielectric bead in an optical trap [82]. Effects of the jumps of the Poisson white noise and the potential function parameters on the mean TPS and the mean TPT in two directions are investigated. To the best of our knowledge this is the first effort to obtain the theoretical results of the mean TPS and the mean TPT of one-dimensional systems driven by Poisson white noise.

The remainder of the paper is structured as follows. In Section 2 we present a general scheme of calculating the solution to the mean TPS and the mean TPT. Section 3, the central part of the paper, is devoted to the specific derivation of the perturbation method to obtain the mean TPS and the mean TPT of one-dimensional systems under Poisson white noise. Section 4 illustrates our approximate theoretical approach for the three mentioned prototypical potential functions. The generalization to multi-state systems on this basis is then straightforward. We use the Forward Flux Sampling (FFS) scheme [83,84] to numerically verify our theoretical approximations for the mean TPS and the mean TPT in these three potentials. Finally, a discussion of the validity of the proposed method and the conclusions are presented in Section 5. Some additional information is provided in the Appendices.

2. Transition path shape and time

We consider the mean TPS and the mean TPT of one-dimensional systems under the driving of Poisson white noise. The system can be described by the stochastic differential equation

$$\frac{dx}{dt} = f(x) + W_p(t), \quad (1)$$

where x is the position of the particle, $f(x) = -dV(x)/dx$ is the force acting on the particle derived from the model potentials $V(x)$ shown in Fig. 1. We consider three simple potential forms: a linear potential, a harmonic ramp, and an inverted parabolic potential. Here the coefficient U controls the height of the potentials $V(x)$.

In Eq. (1), $W_p(t)$ is a Poisson white noise defined as

$$W_p(t) = \sum_{k=1}^{N(t)} Y_k \delta(t - t_k) = \frac{dC(t)}{dt}, \quad (2)$$

which is the formal derivative of the so-called homogeneous compound Poisson process

$$C(t) = \sum_{k=1}^{N(t)} Y_k U_p(t - t_k). \quad (3)$$

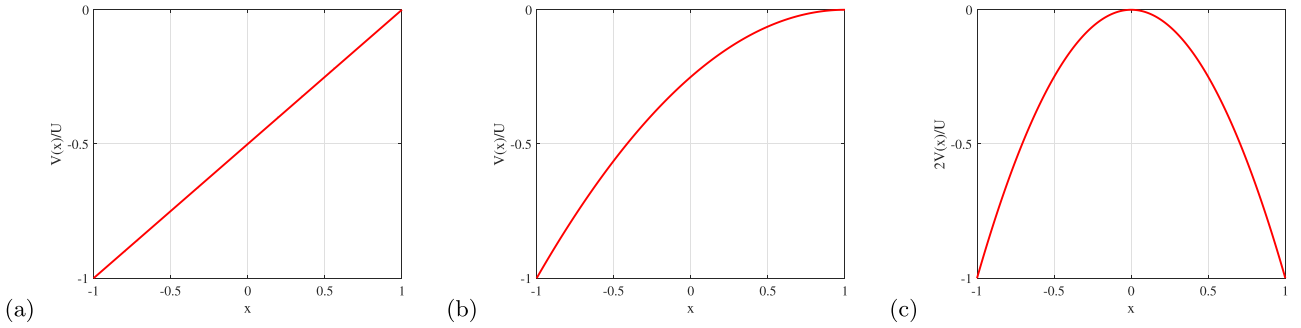


Fig. 1. Potential functions $V(x)$ with the three characteristic shapes considered in this article: (a) linear potential $V(x) = U(x - 1)/2$; (b) harmonic ramp $V(x) = -U(x - 1)^2/4$; (c) inverted parabola $V(x) = -Ux^2/2$.

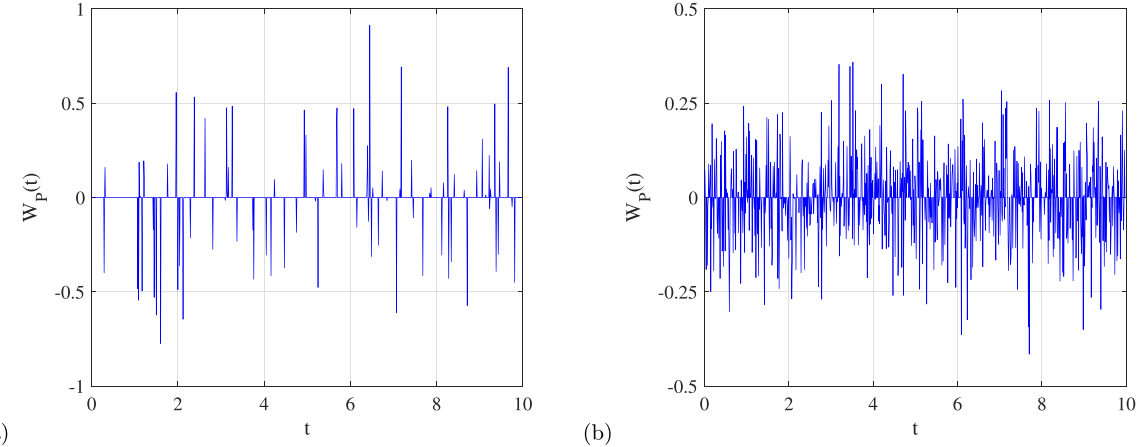


Fig. 2. Poisson white noise $I_0 = 1$ for two different pulse amplitudes: (a) $\mathbb{E}[Y^2] = 0.1$; (b) $\mathbb{E}[Y^2] = 0.01$.

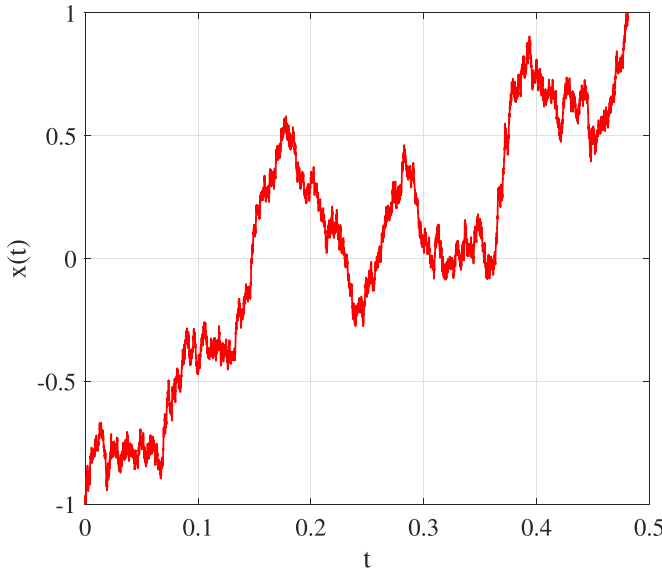


Fig. 3. A transition path is also a first passage path, if $x_A = -1$ and $x_B = 1$ are absorbing boundaries.

Here $\delta(t)$ is the Dirac function, $U_p(t)$ is the unit step function, and $N(t)$ is a Poisson counting process with mean arrival rate λ . Y_k are independent identically distributed random variables, which are independent of the impulse arrival time t_k . The noise intensity of $W_p(t)$ is I_0 , where $I_0 = \lambda \mathbb{E}[Y^2]$. Here Y describes the random pulse amplitude of $W_p(t)$, and $\mathbb{E}[\cdot]$ denotes the expectation of a random variable. In this paper, without loss of generality, we take that Y

obeys the normal distribution $N(0, \sigma^2)$, such that $\mathbb{E}[Y^2] = \sigma^2$. With increase of λ , the number of pulses in the time interval $[0, 10]$ increases, as presented in Fig. 2.

According to the results in [68] the mean TPS $\tau_{\text{shape}}^{\text{TP}}(x_0 | x_A)$ is equal to the mean FPT of particle arriving at x_A from x_0 , under the condition that x_A and x_B are the absorbing boundaries, see the sketch of the setup in Fig. 3. Thus,

$$\tau_{\text{shape}}^{\text{TP}}(x_0 | x_A) = \tau^{\text{FP}}(x_A | x_0), \quad (4)$$

where $[x_A, x_B]$ is the transition path region, and $x_0 \in [x_A, x_B]$. Using this relation the solution of the mean TPS can thus be derived from the mean FPT of the system encoded in Eq. (1). In what follows we define the direction of particle motion from x_A to x_B as the positive direction, otherwise we call it the reverse direction.

The Fokker-Planck equation corresponding to the stochastic equation of motion (1) [85]

$$\frac{\partial}{\partial t} P(x, t | x_0, t_0) = L_{\text{KM}} P(x, t | x_0, t_0), \quad (5)$$

describes the time evolution of the probability density function $P(x, t | x_0, t_0)$. Here L_{KM} is the Fokker-Planck operator, which can be derived from the Kramers-Moyal expansion [85,87], yielding

$$L_{\text{KM}} = -\frac{\partial}{\partial x} [f(x)] - \lambda \mathbb{E}[Y] \frac{\partial}{\partial x} + \frac{\lambda}{2} \mathbb{E}[Y^2] \frac{\partial^2}{\partial x^2} - \frac{\lambda}{6} \mathbb{E}[Y^3] \frac{\partial^3}{\partial x^3} + \frac{\lambda}{24} \mathbb{E}[Y^4] \frac{\partial^4}{\partial x^4} + \dots \quad (6)$$

The splitting probabilities $\phi_A(x)$ and $\phi_B(x)$ then satisfy the relation

$$L_{\text{KM}}^* \phi_A(x) = 0, L_{\text{KM}}^* \phi_B(x) = 0, \quad (7)$$

with the boundary conditions

$$\phi_A(x_A) = 1, \phi_A(x_B) = 0, \phi_B(x_A) = 0, \phi_B(x_B) = 1. \quad (8)$$

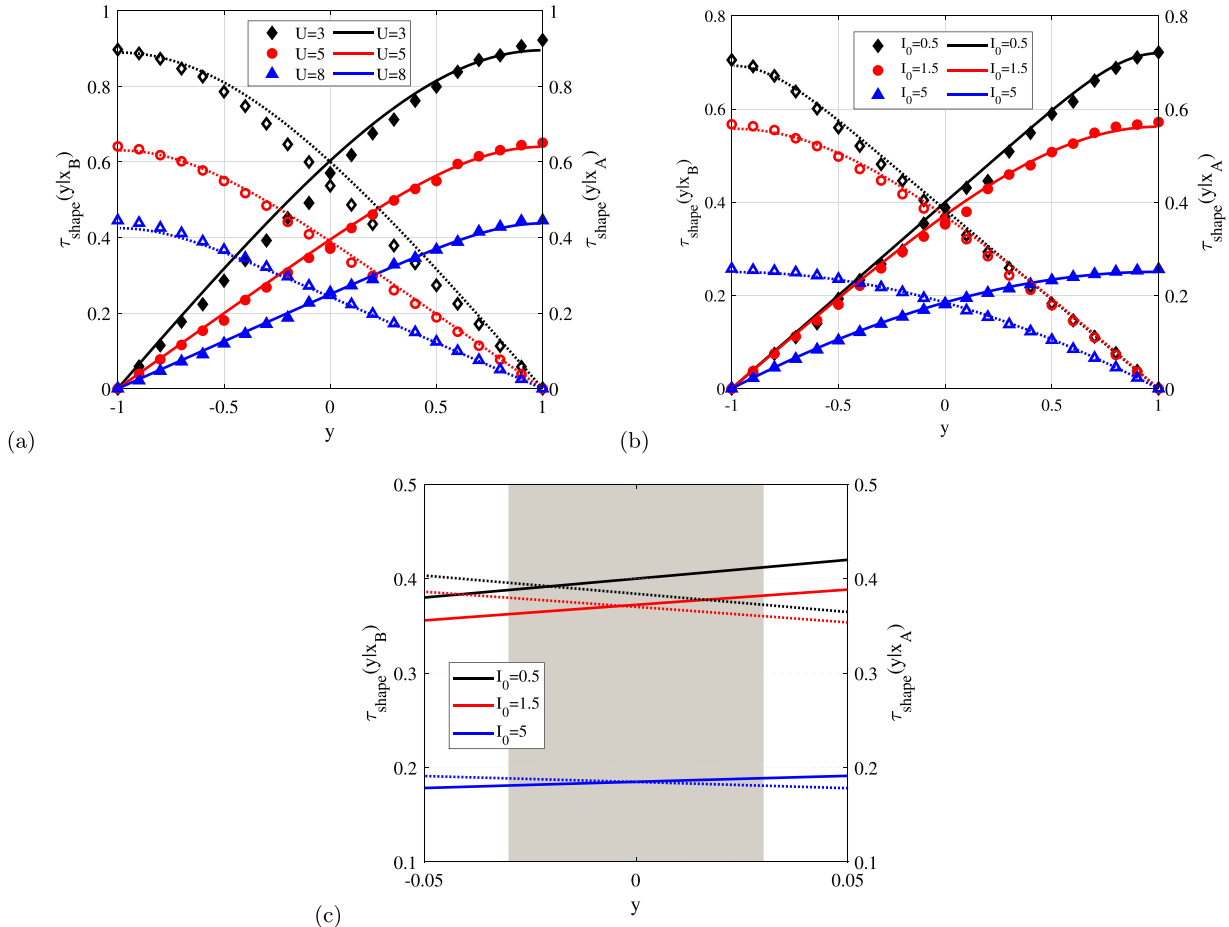


Fig. 4. (a) Mean TPS for different potential heights U , where $I_0 = 1$, $\mathbb{E}[Y^2] = 10^{-3}$. The symbols are defined in the figure panel. (b) Mean TPS for different noise intensities I_0 , where $U = 5$ and $\mathbb{E}[Y^2] = 10^{-3}$. In both panels (a) and (b) symbols represent numerical results from the FFS scheme, while the lines are based on Eq. (38). (c) Theoretical results for the mean TPS for two directions for different I_0 , showing a zoom into panel (b).

L_{KM}^* is the adjoint operator of L_{KM} , and one can show that [87]

$$\begin{aligned} L_{\text{KM}}^* = f(y) \frac{\partial}{\partial y} + \lambda \mathbb{E}[Y] \frac{\partial}{\partial y} + \frac{\lambda}{2} \mathbb{E}[Y^2] \frac{\partial^2}{\partial y^2} + \frac{\lambda}{6} \\ \times \mathbb{E}[Y^3] \frac{\partial^3}{\partial y^3} + \frac{\lambda}{24} \mathbb{E}[Y^4] \frac{\partial^4}{\partial y^4} + \dots, \end{aligned} \quad (9)$$

where y is the backward variable.

We now define $K(x_{A/B}|y)$ as the first-passage distribution of particles from y to x_A or x_B . Consequently, the n th moment of the first-passage distributions is [68]

$$K^{(n)}(x_{A/B}|y) = \int_0^\infty t^n K(x_{A/B}, t|y) dt, \quad (10)$$

and the first passage distributions $K(x_A, t|y)$ and $K(x_B, t|y)$ satisfy

$$\frac{\partial}{\partial t} K(x_{A/B}, t|y) = L_{\text{KM}}^* K(x_{A/B}, t|y). \quad (11)$$

Combining Eqs. (9) and (10) we could obtain the following set of equations [68]

$$-n K^{(n-1)}(x_{A/B}|y) = \int_0^\infty t^n K(x_{A/B}, t|y) dt. \quad (12)$$

Moreover the first passage distributions $K^{(1)}(x_A|y)$ and $K^{(1)}(x_B|y)$ satisfy

$$L_{\text{KM}}^* K^{(1)}(x_{A/B}|y) = -\phi_{A/B}(y). \quad (13)$$

Then the mean FPT is given by

$$\tau^{\text{FP}}(x_{A/B}|y) = \frac{K^{(1)}(x_{A/B}|y)}{\phi_{A/B}(y)}. \quad (14)$$

Thus we need to calculate $\phi_{A/B}(y)$ first, and then combine Eqs. (13) and (14) with Eq. (4) to get the mean TPS encoded by the stochastic differential equation (1).

The mean TPT $\tau^{\text{TP}}(x_A|x_B)$ quantifies the transition path from the absorbing boundary x_B to x_A , its complement $\tau^{\text{TP}}(x_B|x_A)$ is the mean TPT from x_A to x_B . Meanwhile, the mean TPT is the mean FPT of the process (1) from x_B (x_A) to x_A (x_B), i.e., $\tau^{\text{TP}}(x_A|x_B) = \tau^{\text{FP}}(x_A|x_B)$, $\tau^{\text{TP}}(x_B|x_A) = \tau^{\text{FP}}(x_B|x_A)$ with $y \rightarrow x_B$, $y \rightarrow x_A$, respectively. It can be shown that the mean FPT $\tau^{\text{FP}}(x_{A/B}|y)$ is also related to $K^{(1)}(x_{A/B}|y)$ and $\phi_{A/B}(y)$.

3. Approximate solution of the transition path shape and time

Here, we develop the perturbation technique for the approximate solution of the mean TPS of the process (1) driven by Poisson white noise. According to [86,87], without loss of generality, we take $\varepsilon = \lambda^{-1/2}$ as the perturbation parameter. Hence, I_n are finite constants defined as

$$\varepsilon^n I_n = \lambda \mathbb{E}[Y^{n+2}], \quad n = 0, 1, 2, \dots, \quad (15)$$

then Eqs. (7) and (13) turn into

$$f(y) \frac{\partial}{\partial y} \phi_{A/B}(y) + \frac{I_0}{2} \frac{\partial^2}{\partial y^2} \phi_{A/B}(y) + \varepsilon \frac{I_1}{6} \frac{\partial^3}{\partial y^3} \phi_{A/B}(y)$$

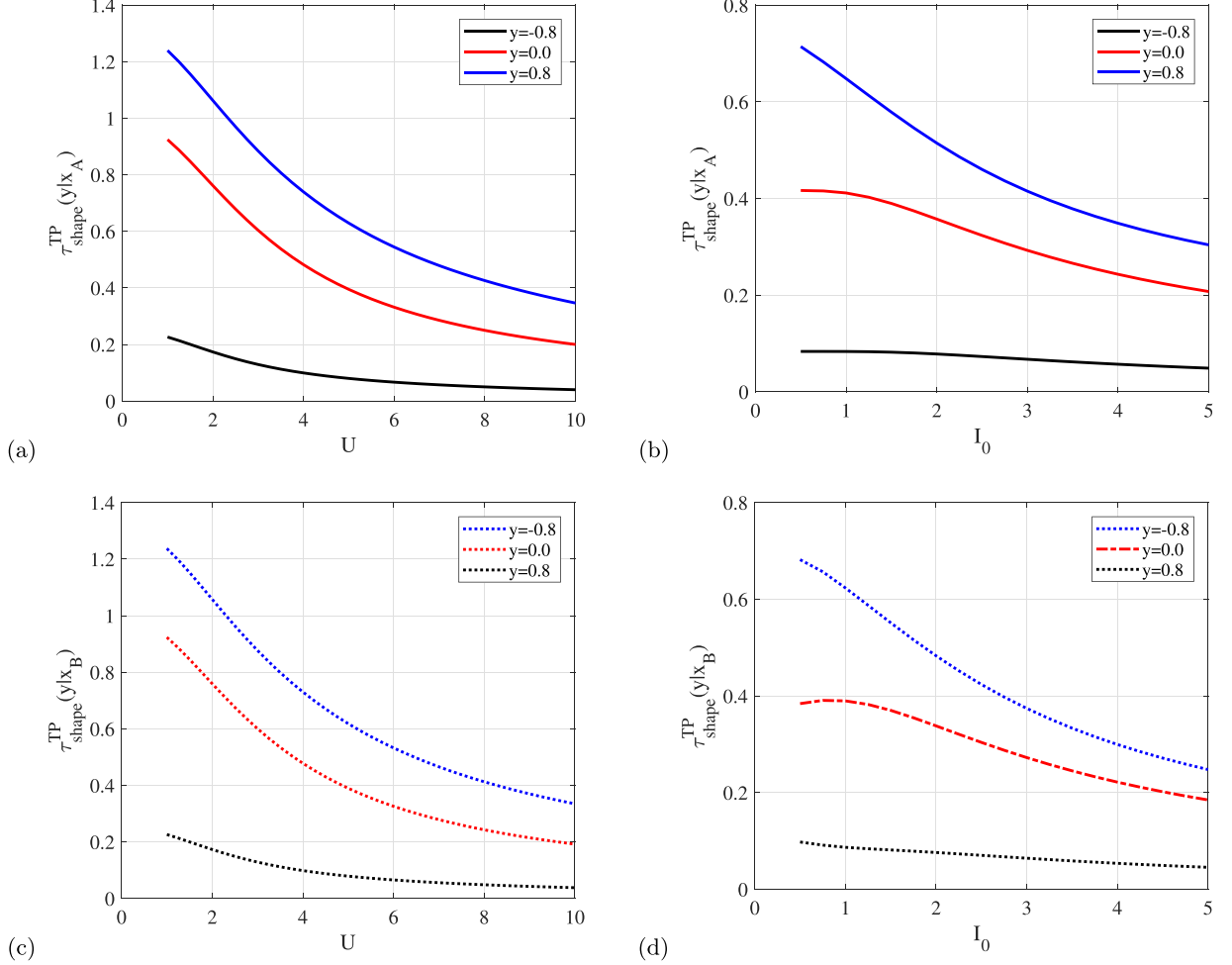


Fig. 5. Theoretical results of the mean TPS $\tau_{\text{shape}}^{\text{TP}}(y|x_A)$ and $\tau_{\text{shape}}^{\text{TP}}(y|x_B)$, $\mathbb{E}[Y^2] = 10^{-3}$. (a, c) $I_0 = 1$, $U \in [1, 10]$; (b, d) $U = 5$, $I_0 \in [0.5, 5]$.

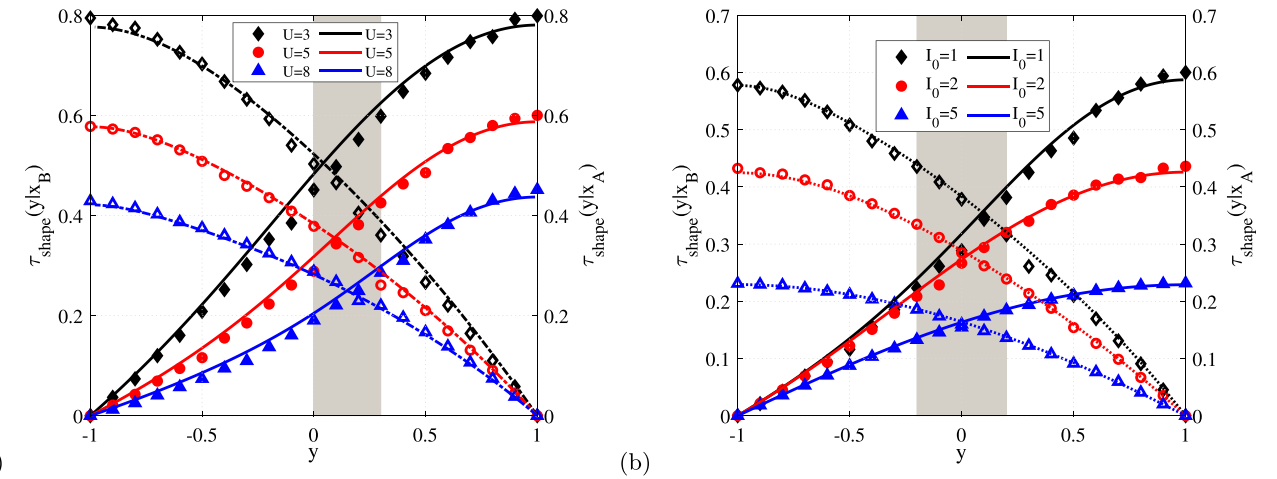


Fig. 6. (a) Mean TPS for different potential heights U , where $I_0 = 1$ and $\mathbb{E}[Y^2] = 10^{-3}$. (b) Mean TPS for different noise intensities I_0 , where $U = 5$ and $\mathbb{E}[Y^2] = 10^{-3}$. The results from the numerical FFS scheme are shown by the symbols, the theoretical results based on Eqs. (38a) and (38b) correspond to the lines.

$$+\varepsilon^2 \frac{I_2}{24} \frac{\partial^4}{\partial y^4} \phi_{A/B}(y) + \dots = 0, \quad (16)$$

$$+\varepsilon^2 \frac{I_2}{24} \frac{\partial^4}{\partial y^4} K^{(1)}(x_{A/B}|y) + \dots = -\phi_{A/B}(y). \quad (17)$$

and

$$f(y) \frac{\partial}{\partial y} K^{(1)}(x_{A/B}|y) + \frac{I_0}{2} \frac{\partial^2}{\partial y^2} K^{(1)}(x_{A/B}|y) + \varepsilon \frac{I_1}{6} \frac{\partial^3}{\partial y^3} K^{(1)}(x_{A/B}|y)$$

Here, we show the detailed derivation of $\phi_A(y)$ and $K^{(1)}(x_A|y)$, while the results for $\phi_B(y)$ and $K^{(1)}(x_B|y)$ are obtained analogously.

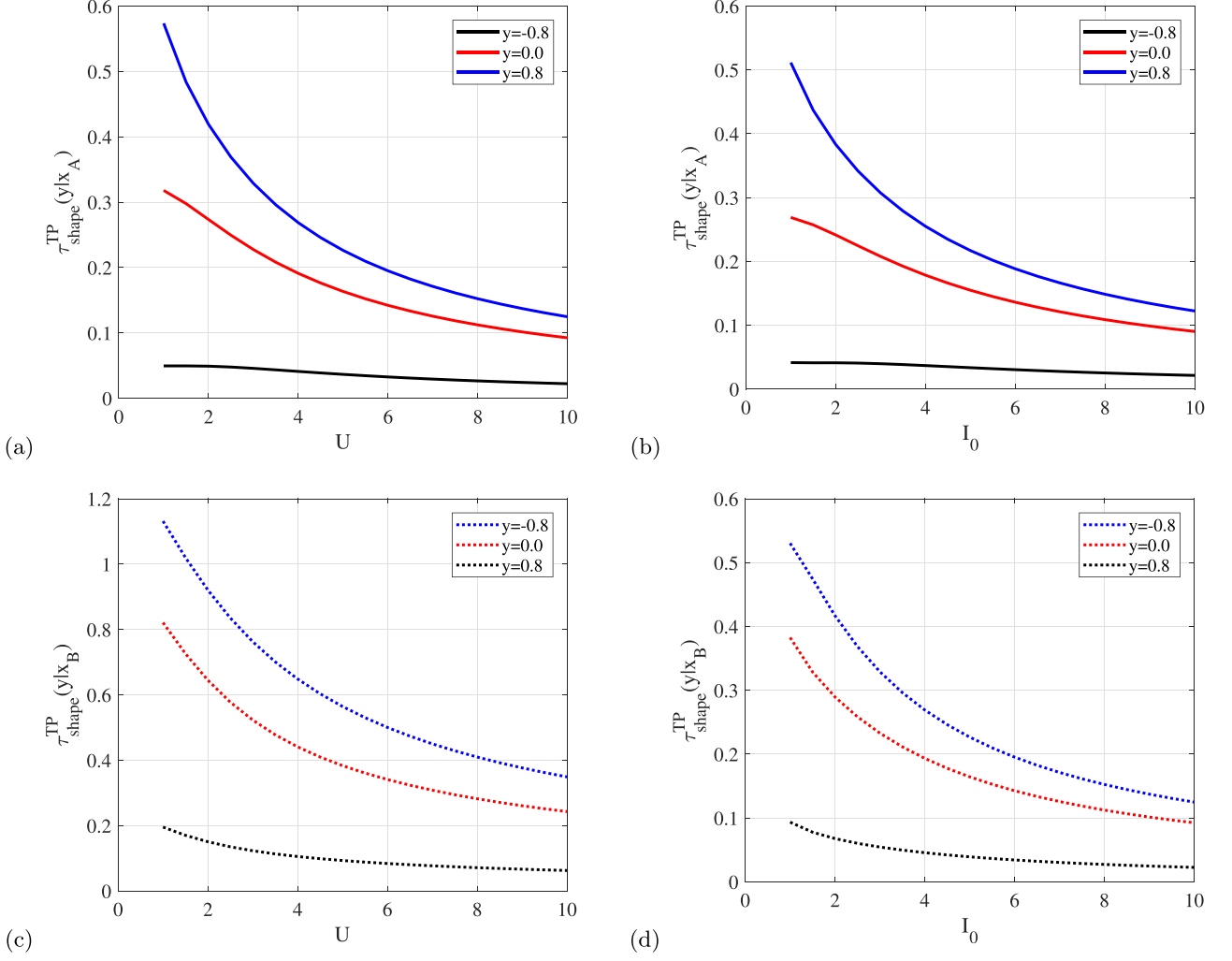


Fig. 7. Theoretical results of the mean TPS $\tau_{\text{shape}}^{\text{TP}}(y|x_A)$ and $\tau_{\text{shape}}^{\text{TP}}(y|x_B)$, $\mathbb{E}[Y^2] = 10^{-3}$. (a, c) $I_0 = 1$, $U \in [1, 10]$; (b, d) $U = 5$, $I_0 \in [1, 10]$.

Suppose that the solution for $\phi_A(y)$ has the form

$$\phi_A(y) = \phi_{A_0}(y) + \varepsilon \phi_{A_1}(y) + \varepsilon^2 \phi_{A_2}(y) + \dots \quad (18)$$

Then substituting Eq. (18) into (16) and grouping terms of the same order in ε , we find

$$\varepsilon^0 : f(y)\phi_{A_0}^{(1)}(y) + \frac{I_0}{2}\phi_{A_0}^{(2)}(y) = 0, \quad (19a)$$

$$\varepsilon^1 : f(y)\phi_{A_1}^{(1)}(y) + \frac{I_0}{2}\phi_{A_1}^{(2)}(y) = -\frac{I_1}{6}\phi_{A_0}^{(3)}(y), \quad (19b)$$

$$\varepsilon^2 : f(y)\phi_{A_2}^{(1)}(y) + \frac{I_0}{2}\phi_{A_2}^{(2)}(y) = -\frac{I_1}{6}\phi_{A_1}^{(3)}(y) - \frac{I_2}{24}\phi_{A_0}^{(4)}(y), \quad (19c)$$

where the $\phi_{A_m}^{(n)}(y)$ denote the n th derivative of $\phi_{A_m}(y)$.

As Y obeys the normal distribution $N(0, \sigma^2)$ we have $I_1 = 0$, and the solution of Eq. (19b) is $\phi_{A_1}(y) = 0$. Therefore, Eqs. (18) to (19c) can be rewritten into

$$\phi_A(y) = \phi_{A_0}(y) + \varepsilon^2 \phi_{A_2}(y) + \dots, \quad (20)$$

and

$$\varepsilon^0 : f(y)\phi_{A_0}^{(1)}(y) + \frac{I_0}{2}\phi_{A_0}^{(2)}(y) = 0, \quad (21a)$$

$$\varepsilon^2 : f(y)\phi_{A_2}^{(1)}(y) + \frac{I_0}{2}\phi_{A_2}^{(2)}(y) = -\frac{I_2}{24}\phi_{A_0}^{(4)}(y). \quad (21b)$$

According to the boundary condition (8) we obtain

$$\phi_{A_0}(y) = \frac{\int_y^{x_B} e^{\frac{2}{I_0}V(s)} ds}{\int_{x_A}^{x_B} e^{\frac{2}{I_0}V(s)} ds}, \quad (22a)$$

$$\begin{aligned} \phi_{A_2}(y) &= \phi_{A_0}(x) \int_{x_A}^y \int_x^{x_B} \frac{2}{I_0} g_1(s) e^{-\frac{2}{I_0}V(s)} ds e^{\frac{2}{I_0}V(x)} dx \\ &\quad - \phi_{B_0}(x) \int_y^{x_B} \int_x^{x_B} \frac{2}{I_0} g_1(s) e^{-\frac{2}{I_0}V(s)} ds e^{\frac{2}{I_0}V(x)} dx \\ &= \phi_{A_0}(y)N_1(y) - \phi_{B_0}(y)N_2(y), \end{aligned} \quad (22b)$$

where $g_1(x) = (I_2/24)\phi_{A_0}^{(4)}(x)$. Then combining Eq. (20) with Eqs. (22) we get $\phi_A(y)$.

Next we assume that the solution $K^{(1)}(x_A|y)$ is of the form

$$K^{(1)}(x_A|y) = K_0^{(1)}(x_A|y) + \varepsilon K_1^{(1)}(x_A|y) + \varepsilon^2 K_2^{(1)}(x_A|y) + \dots \quad (23)$$

Combination with Eq. (17) leads to the set of equations

$$\varepsilon^0 : f(y)K_0^{(1)(1)}(x_A|y) + \frac{I_0}{2}K_0^{(1)(2)}(x_A|y) = 0, \quad (24a)$$

$$\varepsilon^1 : f(y)K_1^{(1)(1)}(x_A|y) + \frac{I_0}{2}K_1^{(1)(2)}(x_A|y) = -\frac{I_1}{6}K_0^{(1)(3)}(x_A|y), \quad (24b)$$

$$\varepsilon^2 : f(y)K_2^{(1)(1)}(x_A|y) + \frac{I_0}{2}K_2^{(1)(2)}(x_A|y)$$

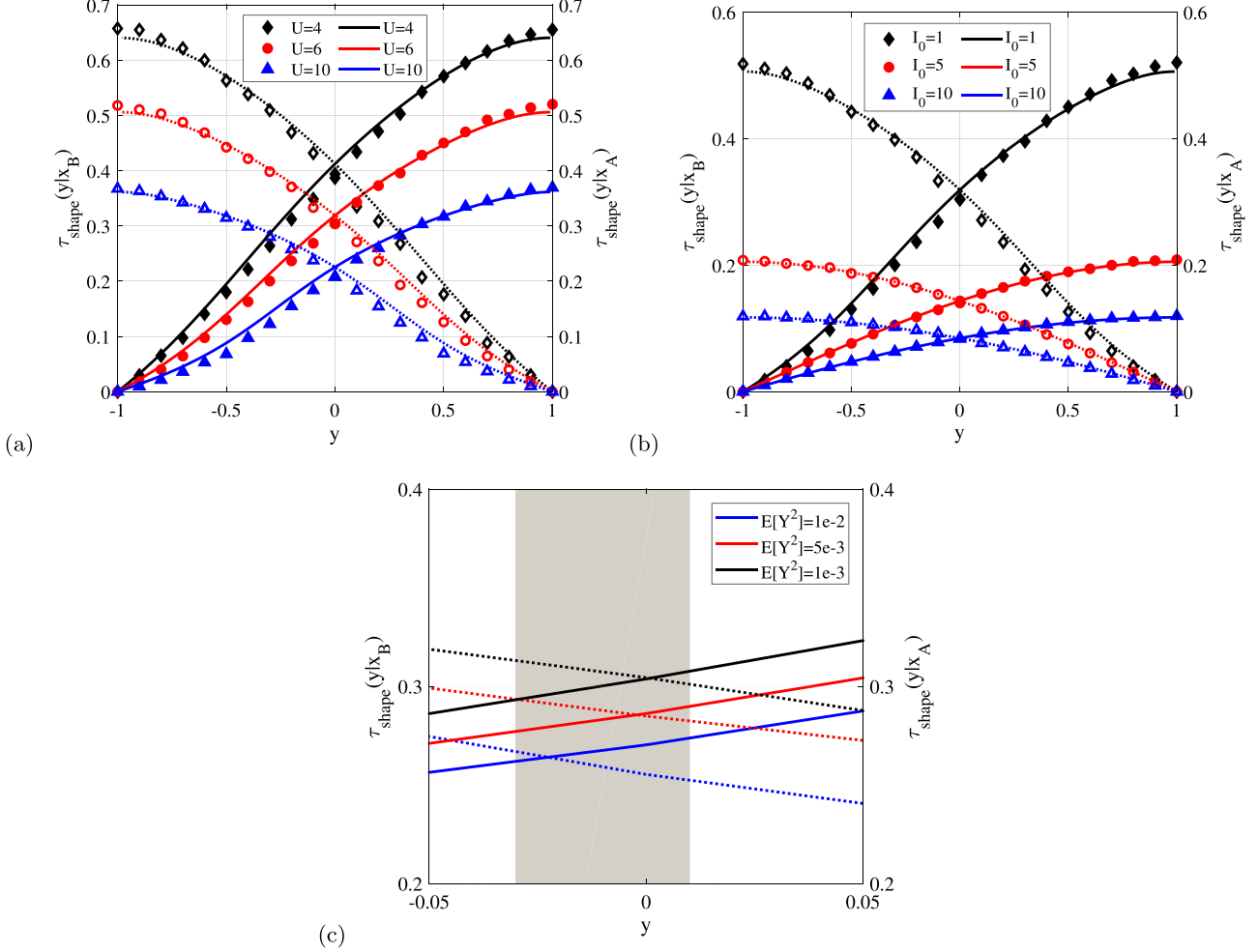


Fig. 8. (a) Mean TPS for different potential height U , where $I_0 = 1$ and $\mathbb{E}[Y^2] = 10^{-3}$. (b) Mean TPS for different noise intensities I_0 , where $U = 6$ and $\mathbb{E}[Y^2] = 10^{-3}$. (c) Simulation results for the mean TPS for the two transition directions. Results from the FFS scheme are shown by symbols, lines depict the behavior encoded in Eqs. (38a) and (38b).

$$= -\frac{I_1}{6} K_1^{(1)(3)}(x_A|y) - \frac{I_2}{24} K_0^{(1)(4)}(x_A|y), \quad (24c)$$

where $K_m^{(1)(n)}(x_A|y)$ is the n th derivative of $K_m^{(1)}(x_A|y)$.

Since $Y \sim N(0, \sigma^2)$, we see that $K_1^{(1)}(x_A|y) = 0$ and Eqs. (23) and (24) can be simplified to

$$K^{(1)}(x_A|y) = K_0^{(1)}(x_A|y) + \varepsilon^2 K_2^{(1)}(x_A|y) + \dots, \quad (25)$$

and

$$\varepsilon^0 : f(y) K_0^{(1)(1)}(x_A|y) + \frac{I_0}{2} K_0^{(1)(2)}(x_A|y) = 0, \quad (26a)$$

$$\varepsilon^2 : f(y) K_2^{(1)(1)}(x_A|y) + \frac{I_0}{2} K_2^{(1)(2)}(x_A|y) = -\frac{I_2}{24} K_0^{(1)(4)}(x_A|y). \quad (26b)$$

Therefore,

$$\begin{aligned} K_0^{(1)}(x_A|y) &= \phi_{A_0}(y) \int_{x_A}^y \int_x^{x_B} \frac{2}{I_0} \phi_{A_0}(s) e^{-\frac{2}{I_0} V(s)} ds e^{\frac{2}{I_0} V(x)} dx \\ &\quad - \phi_{B_0}(y) \int_y^{x_B} \int_x^{x_B} \frac{2}{I_0} \phi_{A_0}(s) e^{-\frac{2}{I_0} V(s)} ds e^{\frac{2}{I_0} V(x)} dx \\ &= \phi_{A_0}(y) M_{11}(y) - \phi_{B_0}(y) M_{12}(y), \end{aligned} \quad (27a)$$

$$K_2^{(1)}(x_A|y) = \phi_{A_0}(y) \int_{x_A}^y \int_x^{x_B} \frac{2}{I_0} G_1(s) e^{-\frac{2}{I_0} V(s)} ds e^{\frac{2}{I_0} V(x)} dx$$

$$\begin{aligned} &- \phi_{B_0}(y) \int_y^{x_B} \int_x^{x_B} \frac{2}{I_0} G_1(s) e^{-\frac{2}{I_0} V(s)} ds e^{\frac{2}{I_0} V(x)} dx \\ &= \phi_{A_0}(y) M_{21}(y) - \phi_{B_0}(y) M_{22}(y), \end{aligned} \quad (27b)$$

where $G_1(y) = \phi_{A_2}(y) + \frac{I_2}{24} K_0^{(1)(4)}(x_A|y)$, and $K_0^{(1)(4)}(x_A|y)$ is the fourth derivative of $K_0^{(1)}(x_A|y)$.

Then, substituting $K_0^{(1)}(x_A|y)$ and $K_2^{(1)}(x_A|y)$ into Eq. (25) one can obtain the first-passage distribution $K^{(1)}(x_A|y)$. The mean TPS can be derived from Eq. (4),

$$\tau_{\text{shape}}^{\text{TP}}(y|x_A) = \tau^{\text{FP}}(x_A|y) \approx \frac{K_0^{(1)}(x_A|y) + \varepsilon^2 K_2^{(1)}(x_A|y)}{\phi_{A_0}(y) + \varepsilon^2 \phi_{A_2}(y)}, \quad (28)$$

then combining Eq. (22) with Eq. (27) we obtain

$$\tau_{\text{shape}}^{\text{TP}}(y|x_A) = \tau^{\text{FP}}(x_A|y) \approx \frac{H_1(y) + \varepsilon^2 H_2(y)}{1 + \varepsilon^2 [N_1(y) - C_1(y)N_2(y)]}, \quad (29)$$

where $C_1(y) = \frac{\phi_{B_0}(y)}{\phi_{A_0}(y)}$, $H_1(y) = M_{11}(y) - C_1(y)M_{12}(y)$, and $H_2(y) = M_{21}(y) - C_1(y)M_{22}(y)$.

Moreover, according to Eq. (14) when $y \rightarrow x_B$,

$$\tau^{\text{TP}}(x_A|x_B) = \tau^{\text{FP}}(x_A|y \rightarrow x_B) \approx \frac{M_{11}(x_B) + \varepsilon^2 M_{21}(x_B)}{1 + \varepsilon^2 N_1(x_B)}. \quad (30)$$

Since we want to compare the mean TPS and the mean TPT in the two directions, as $Y \sim N(0, \sigma^2)$ the splitting probability $\phi_B(y)$

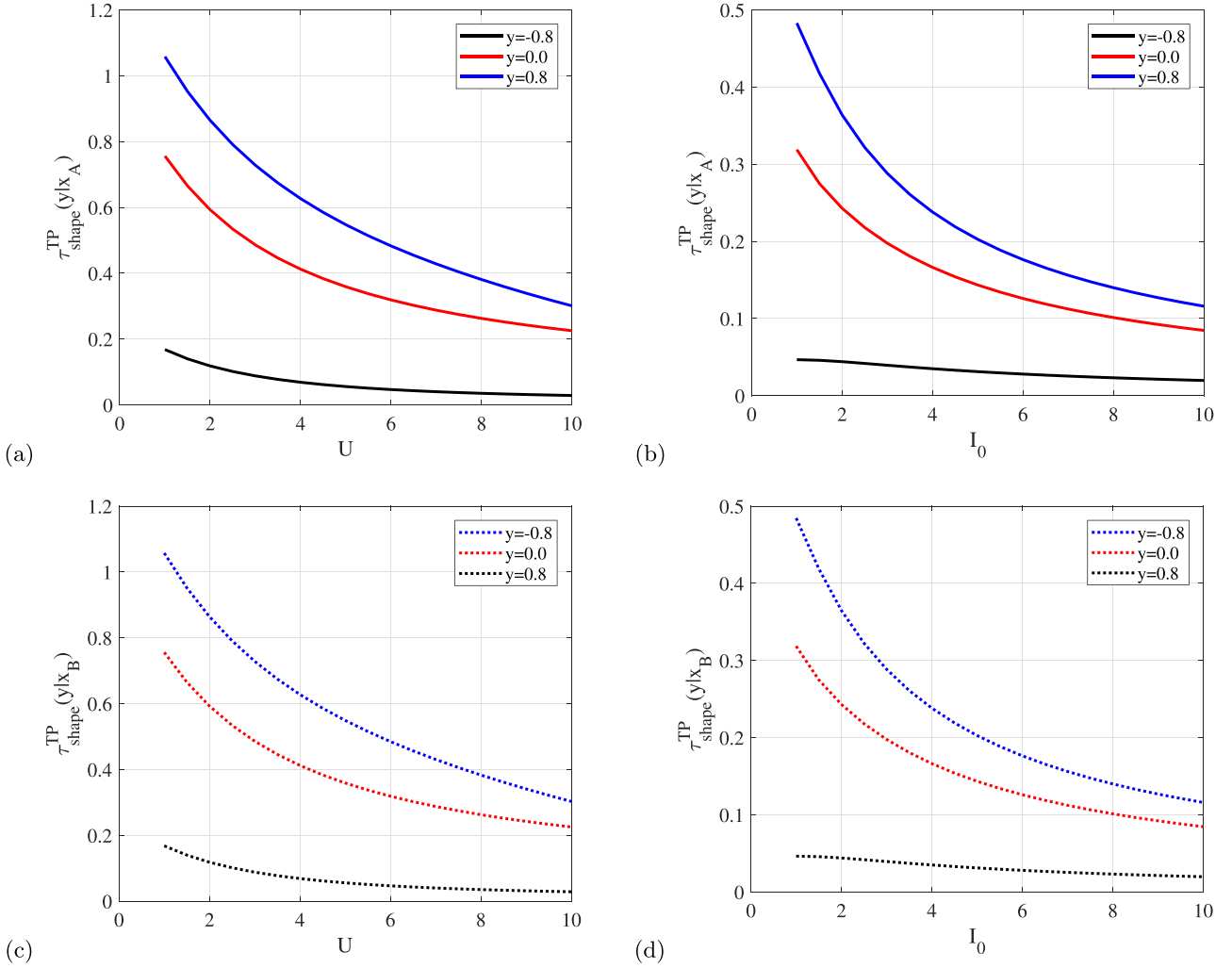


Fig. 9. Theoretical results of mean TPS $\tau_{\text{shape}}^{\text{TP}}(y|x_A)$ and $\tau_{\text{shape}}^{\text{TP}}(y|x_B)$, $\mathbb{E}[Y^2] = 10^{-3}$. (a, c) $I_0 = 1$, $U \in [1, 10]$; (b, d) $U = 6$, $I_0 \in [1, 10]$.

is assumed to obey

$$\phi_B(x) = \phi_{B_0}(y) + \varepsilon^2 \phi_{B_2}(y) + \dots \quad (31)$$

Substituting this form into Eq. (7) and combining with the boundary condition (8) we get

$$\phi_{B_0}(y) = \frac{\int_{x_A}^y e^{\frac{2}{l_0}V(s)} ds}{\int_{x_A}^{x_B} e^{\frac{2}{l_0}V(s)} ds}, \quad (32a)$$

$$\begin{aligned} \phi_{B_2}(y) &= \phi_{B_0}(y) \int_y^{x_B} \int_{x_A}^x \frac{2}{l_0} g_2(s) e^{-\frac{2}{l_0}V(s)} ds e^{\frac{2}{l_0}V(x)} dx \\ &\quad - \phi_{A_0}(y) \int_{x_A}^y \int_{x_A}^x \frac{2}{l_0} g_2(s) e^{-\frac{2}{l_0}V(s)} ds e^{\frac{2}{l_0}V(x)} dx, \\ &= \phi_{B_0}(y) \bar{N}_1(y) - \phi_{A_0}(y) \bar{N}_2(y), \end{aligned} \quad (32b)$$

where $g_2(y) = \frac{l_2}{24} \phi_{B_0}^{(4)}(y)$, and $\phi_{B_0}^{(n)}(y)$ denotes the n th derivative of $\phi_{B_0}(y)$.

Similarly, we assume that

$$K^{(1)}(x_B|y) = K_0^{(1)}(x_B|y) + \varepsilon^2 K_2^{(1)}(x_B|y) + \dots \quad (33)$$

This leads us to

$$\begin{aligned} K_0^{(1)}(x_B|y) &= \phi_{B_0}(y) \int_y^{x_B} \int_{x_A}^x \frac{2}{l_0} \phi_{B_0}(s) e^{-\frac{2}{l_0}V(s)} ds e^{\frac{2}{l_0}V(x)} dx \\ &\quad - \phi_{A_0}(y) \int_{x_A}^y \int_{x_A}^x \frac{2}{l_0} \phi_{B_0}(s) e^{-\frac{2}{l_0}V(s)} ds e^{\frac{2}{l_0}V(x)} dx, \end{aligned}$$

$$= \phi_{B_0}(y) \bar{M}_{11}(y) - \phi_{A_0}(y) \bar{M}_{12}(y), \quad (34a)$$

$$\begin{aligned} K_2^{(1)}(x_B|y) &= \phi_{B_0}(y) \int_y^{x_B} \int_{x_A}^x \frac{2}{l_0} G_2(s) e^{-\frac{2}{l_0}V(s)} ds e^{\frac{2}{l_0}V(x)} dx \\ &\quad - \phi_{A_0}(y) \int_{x_A}^y \int_{x_A}^x \frac{2}{l_0} G_2(s) e^{-\frac{2}{l_0}V(s)} ds e^{\frac{2}{l_0}V(x)} dx \\ &= \phi_{B_0}(y) \bar{M}_{21}(y) - \phi_{A_0}(y) \bar{M}_{22}(y), \end{aligned} \quad (34b)$$

where $G_2(y) = \phi_{B_2}(y) + (l_2/24) K_0^{(1)(4)}(x_B|y)$, and $K_0^{(1)(4)}(x_B|y)$ is the fourth derivative of $K_0^{(1)}(x_B|y)$. Then the mean TPS of particle from x_B to y is

$$\tau_{\text{shape}}^{\text{TP}}(y|x_B) = \tau^{\text{FP}}(x_B|y) \approx \frac{K_0^{(1)}(x_B|y) + \varepsilon^2 K_2^{(1)}(x_B|y)}{\phi_{B_0}(y) + \varepsilon^2 \phi_{B_2}(y)}. \quad (35)$$

then combining Eq. (32b) with Eq. (34) one has

$$\tau_{\text{shape}}^{\text{TP}}(y|x_B) \approx \frac{\bar{H}_1(y) + \varepsilon^2 \bar{H}_2(y)}{1 + \varepsilon^2 [\bar{N}_1(y) - C_2(y) \bar{N}_2(y)]}, \quad (36)$$

where $C_2(y) = \frac{\phi_{A_0}(y)}{\phi_{B_0}(y)}$, $\bar{H}_1(y) = \bar{M}_{11}(y) - C_2(y) \bar{M}_{12}(y)$, and $\bar{H}_2(y) = \bar{M}_{21}(y) - C_2(y) \bar{M}_{22}(y)$.

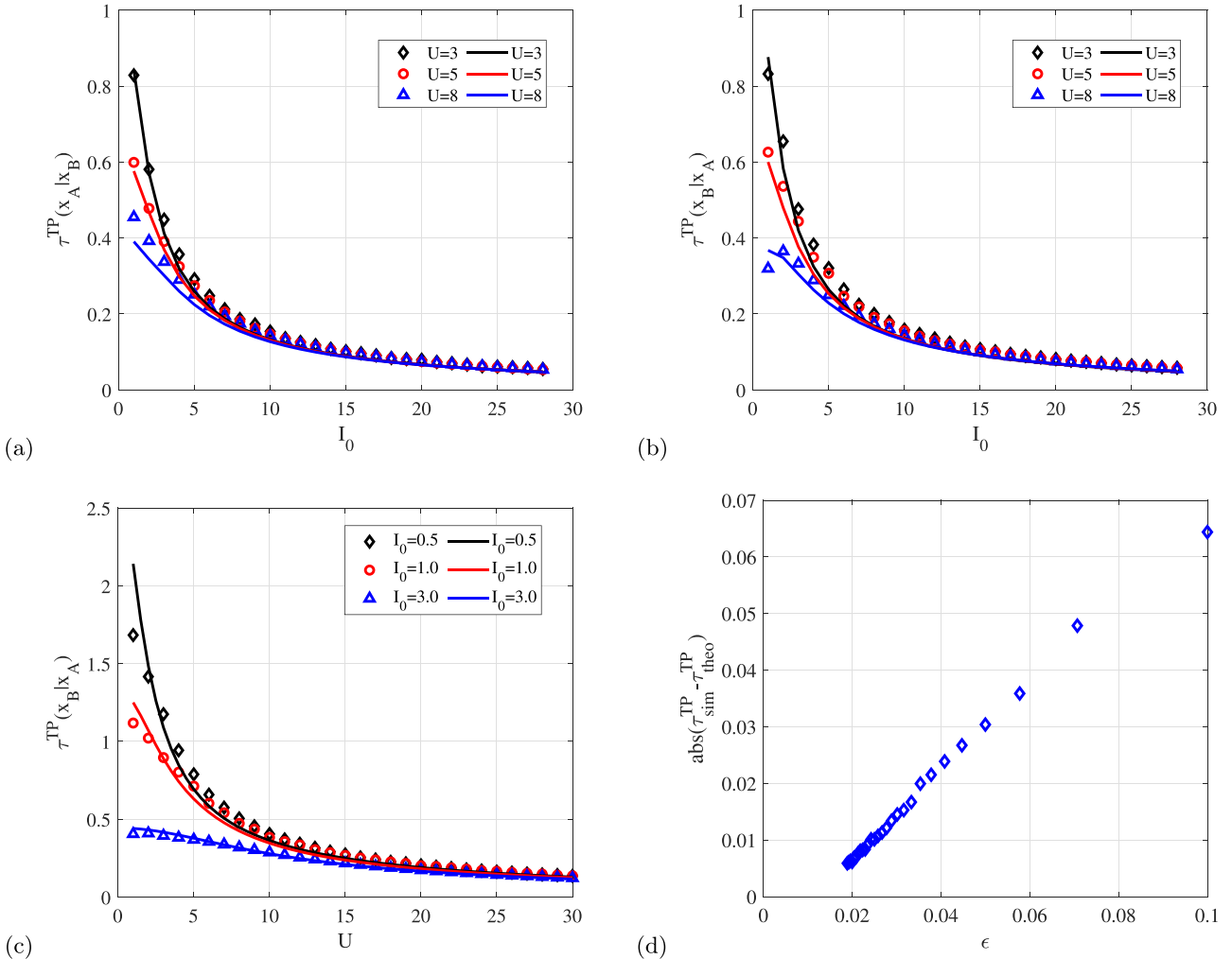


Fig. 10. (a) Mean TPT $\tau^{\text{TP}}(x_B|x_A)$ for transitions from x_B to x_A for different potential heights U , where $I_0 \in [1, 28]$ and $\mathbb{E}[Y^2] = 10^{-2}$; (b) Mean TPT $\tau^{\text{TP}}(x_A|x_B)$ for transitions from x_A to x_B for different potential heights U , where $I_0 \in [1, 28]$ and $\mathbb{E}[Y^2] = 10^{-2}$; (c) $\tau^{\text{TP}}(x_B|x_A)$ changes with U , where $U \in [1, 30]$ and $\mathbb{E}[Y^2] = 10^{-3}$; in (a), (b) and (c) the symbols represent numerical results from the FFS scheme, lines represent the theoretical results (30) and (37). (d) Error of the mean TPT between numerical and theoretical results as function of the perturbation parameter ϵ .

Similarly, when $y \rightarrow x_A$ the mean TPT from x_A to x_B can therefore be approximated by

$$\tau^{\text{TP}}(x_B|x_A) = \tau^{\text{FP}}(x_B|y \rightarrow x_A) \approx \frac{\bar{M}_{11}(x_A) + \varepsilon^2 \bar{M}_{21}(x_A)}{1 + \varepsilon^2 \bar{N}_1(x_A)}. \quad (37)$$

We thus obtained the theoretical results for the mean TPS and the mean TPT of a particle moving from y to x_A as shown in Eqs. (29) and (30), and Eqs. (36) and (37) are the approximate results of the mean TPS and the mean TPT in the opposite direction.

4. Results

4.1. Mean transition path shape

4.1.1. Linear potential

To illustrate the theoretical approach introduced in the previous section and to verify the correctness of our approximation scheme we study the application to the three simple potential functions shown in Fig. 1. In this paper, the FFS scheme is applied to verify our proposed approximation approach. First, we obtain the mean TPS of a stochastically moving particle in a linear potential function $V(x) = U(x - 1)/2$ represented in Fig. 1(a) under the action of

Poisson white noise. From the above perturbation scheme we obtain the concrete form of the mean TPS in the two directions, see Eqs. (28) and (35), respectively. The main terms in these equations are

$$\begin{aligned} M_{11}(y) = & \frac{2}{cl_0} \left[\frac{I_0}{U} y e^{\frac{U}{l_0} y} - \frac{I_0}{U} \left(1 + \frac{2l_0}{U} \right) e^{\frac{U}{l_0} y} \right. \\ & \left. + \frac{I_0}{U} e^{\frac{U}{l_0} (y+1)} + \frac{2l_0}{U} \left(1 + \frac{l_0}{U} \right) e^{-\frac{U}{l_0} y} \right], \end{aligned} \quad (38a)$$

and

$$\begin{aligned} \bar{M}_{11}(y) = & \frac{2}{cl_0} \left[-\frac{I_0}{U} y e^{\frac{U}{l_0} y} + \frac{I_0}{U} \left(\frac{2l_0}{U} - 1 \right) e^{\frac{U}{l_0} y} \right. \\ & \left. + \frac{I_0}{U} e^{-\frac{U}{l_0} (y+1)} + \frac{2l_0}{U} \left(1 - \frac{l_0}{U} \right) e^{\frac{U}{l_0} y} \right], \end{aligned} \quad (38b)$$

while the other terms are presented in Appendix A.

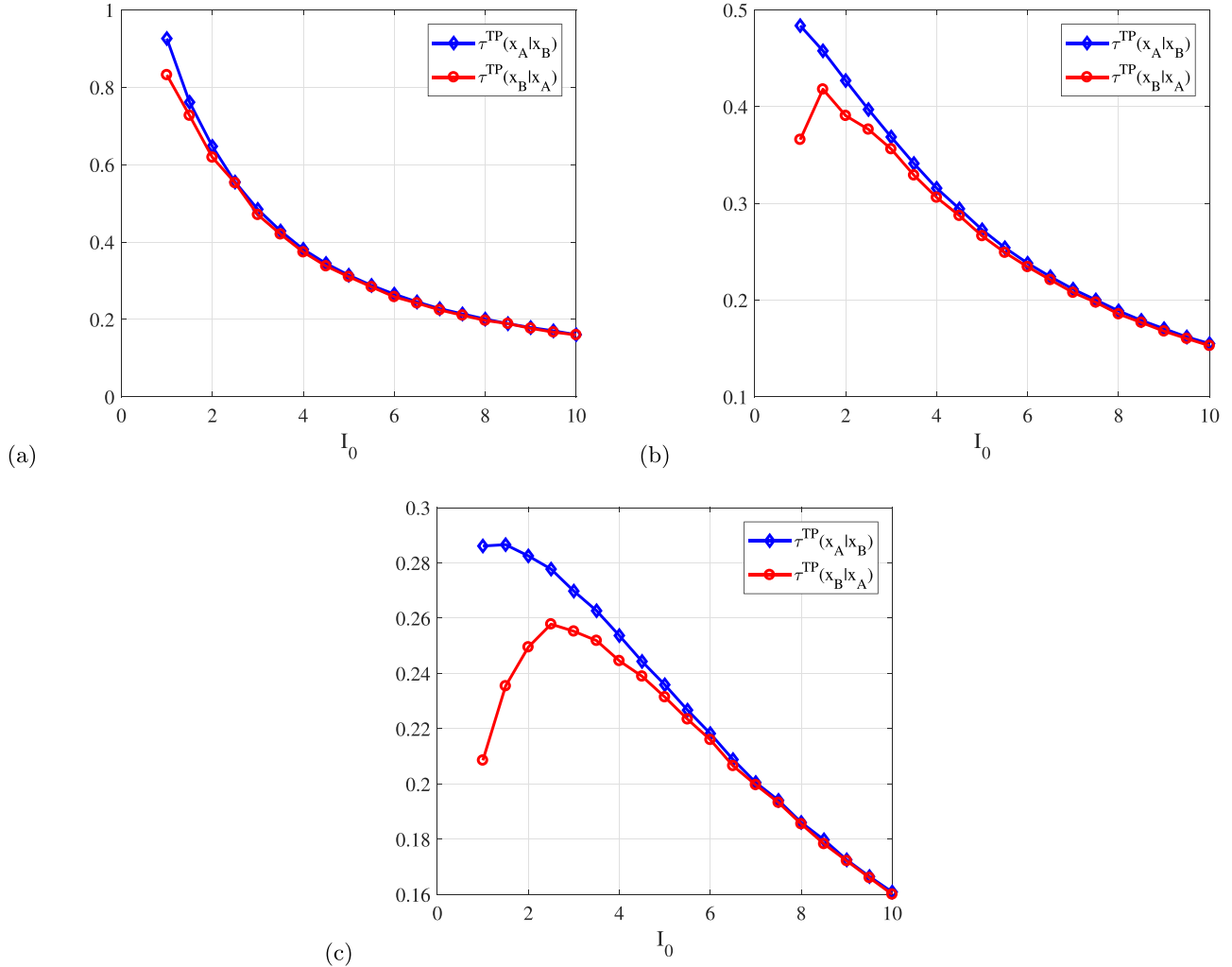


Fig. 11. Comparisons of the mean TPT for transition paths from x_B to x_A and x_A to x_B , respectively, from Fig. 6, with $E[Y^2] = 10^{-2}$ and $I_0 \in [1, 10]$. We show results for three different barrier heights, (a) $U = 3$, (b) $U = 8$, and (c) $U = 15$.

The numerical results for $\tau_{\text{shape}}^{\text{TP}}(y|x_A)$ and $\tau_{\text{shape}}^{\text{TP}}(y|x_B)$ confirm the accuracy of our approximate theoretical predictions for the mean TPS shown in Eqs. (28) and (35), as illustrated in Fig. 4. Note the complex way in which the potential height U enters these expressions.

The mean TPS for various potential heights U and noise intensity I_0 is shown in Fig. 4(a) and 4(b), corresponding to the two directions of transition paths, respectively. Fig. 4(a) shows that the mean TPS increases with decreasing potential height, in accordance with results (38a) and (38b). It also shows that the noise intensity has a beneficial effect, such that higher noise intensity effects shorter mean TPS. A similar phenomenon can be observed in the Fig. 5. We also see that the numerical results from the FFS scheme nicely verify the approximate theoretical results. The difference between the theoretical and numerical results decreases with increase of U . Remarkably, the mean TPS of the system in the two directions is indeed symmetrical for the parameters in Fig. 4(a). We note that in all examples the maximum of the mean TPS curves are located right at the interval boundaries x_A or x_B . This is a feature that is consistent for all examples considered here. In order to further detail the effect of the noise intensity on the mean TPS, in Fig. 4(c) we zoom into the central region of panel 4(b). We see that with increasing noise intensity I_0 the asymmetry of the mean TPS in forward and backward directions becomes increasingly distinct (both with respect to the crossing points and

the amplitude difference between the two larger noise intensities). This is in fact a remarkable outcome for the mean TPS $\tau_{\text{shape}}^{\text{TP}}(y|x_A)$ and $\tau_{\text{shape}}^{\text{TP}}(y|x_B)$: the noise intensity of Poisson white noise alters the symmetry of the mean TPS with respect to forward/backward transitions, while the symmetry is fulfilled for any noise intensity in the case of Gaussian white noise sources. Note that for better visibility we only show the theoretical result in panel 4(c), for the two different directions, without the numerical results, as Fig. 4(b) demonstrates that theoretical and numerical results are in good agreement.

According to Eqs. (29) and (36), it is clear that a bigger U or I_0 results to a smaller mean TPS as shown in Fig. 5.

4.1.2. Harmonic ramp

We proceed to study the mean TPS for the harmonic ramp potential $V(x) = -U(x-1)^2/4$ shown in Fig. 1(b). The numerical FFS simulations for the stochastic process (1) are compared to our approximate theoretical results in Eqs. (28) and (35). As Fig. 6 demonstrates the general behavior is similar to the linear potential case considered previously. Namely, the mean TPS decreases with increasing potential height U and decreases with increasing noise intensity I_0 . Concurrently the agreement between the numerical results and our approximate theory becomes increasingly better as the height of potential U or the amplitude of the noise intensity I_0 grow. In Fig. 6(a) we show the effect of the potential

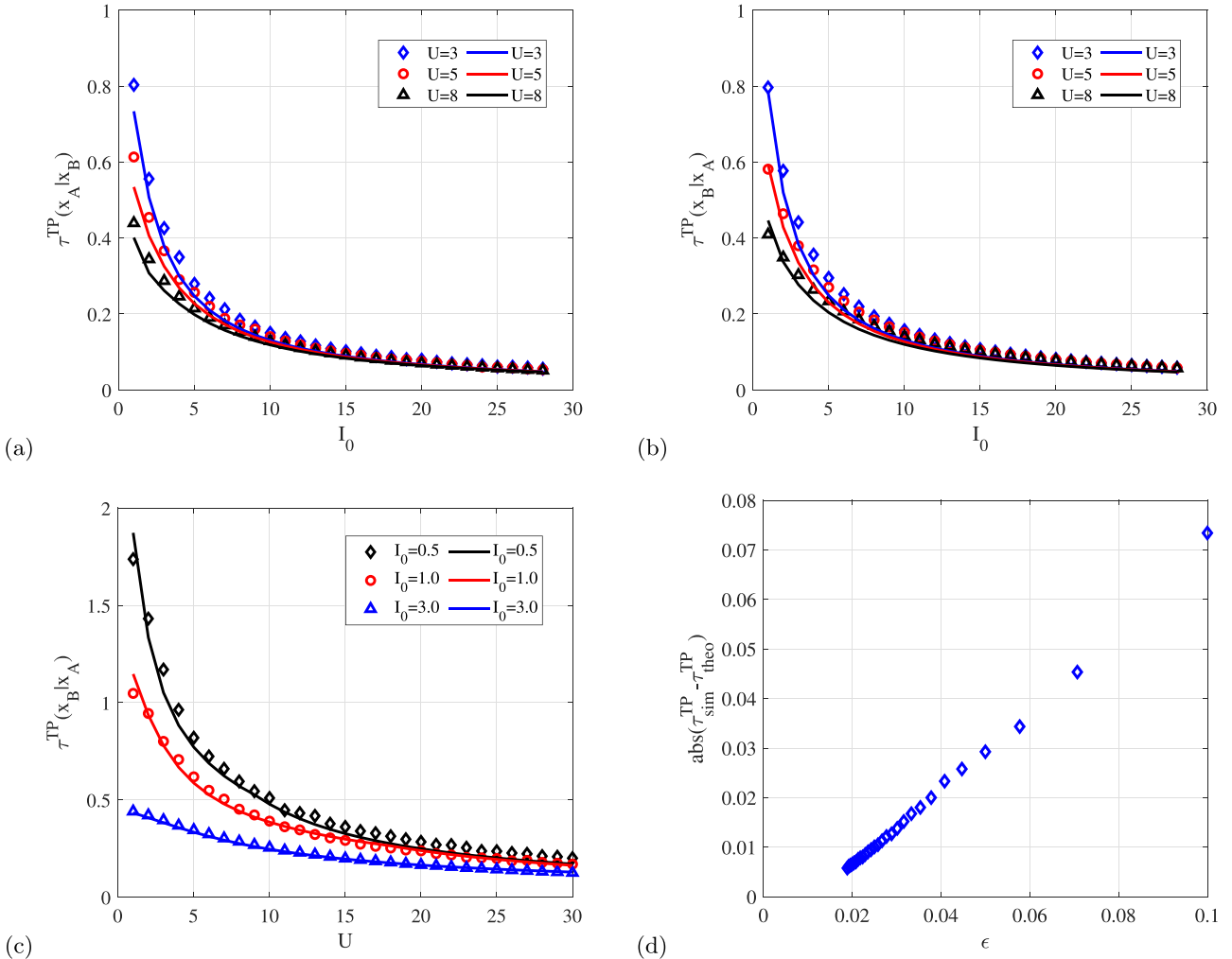


Fig. 12. (a) Mean TPT $\tau^{TP}(x_A|x_B)$ for transition paths from x_B to x_A , for $I_0 \in [1, 28]$ and $\mathbb{E}[Y^2] = 10^{-2}$; (b) Mean TPT $\tau^{TP}(x_B|x_A)$ for transitions from x_A to x_B , for $I_0 \in [1, 28]$ and $\mathbb{E}[Y^2] = 10^{-2}$; (c) $\tau^{TP}(x_B|x_A)$ changes with U , where $U \in [1, 30]$ and $\mathbb{E}[Y^2] = 10^{-3}$. In these panels symbols represent numerical results from the FFS scheme, while lines represent the theoretical approximation based on Eqs. (30) and (37). (d) Absolute deviation between the theoretical and numerical results for the mean TPT.

height on the mean TPS. We observe that the mean TPS for the two directions become more asymmetric with increasing barrier height. As illustrated in Fig. 6(b), the mean TPS as a function of noise intensity increases with decreasing I_0 for both directions. Moreover, with decreasing noise intensity the asymmetry of the mean TPS becomes more pronounced as shown in the shaded part of panel 6(b). In both panels of Fig. 6 the agreement between the numerical FFS results and the theoretical approximation is very nice for all parameters.

In Fig. 7 we show the influence of U and I_0 on the $\tau_{shape}^{TP}(y|x_A)$ and $\tau_{shape}^{TP}(y|x_B)$. With the increase of U or I_0 , both $\tau_{shape}^{TP}(y|x_A)$ and $\tau_{shape}^{TP}(y|x_B)$ show a decreasing trend. This also verifies the phenomenon shown in Fig. 6.

4.1.3. Inverted parabolic potential

Another paradigmatic case is the inverted parabolic potential $V(x) = -Ux^2/2$, which corresponds to Fig. 1(c). To check the influence of the potential height and the noise intensity on the statistics of the mean TPS for this example, we show the FFS numerical results along with the theoretical approximation in Fig. 8. Overall very nice agreement is observed. When the potential height U decreases the mean TPS increases, while it increases with decreasing noise intensity I_0 , as revealed in panels 8(a) and 8(b).

In Figs. 8(a) and 8(b) the effect of the barrier height and the noise intensity on the asymmetry of the mean TPS cannot be clearly observed. Therefore, it is necessary to reduce the perturbation parameter to examine the symmetry of the mean TPS in more detail. In Fig. 8(c) we can see that, as the perturbation parameter ϵ decreases, the asymmetry of the mean TPS becomes more significant. Furthermore, the error of the approximate theoretical result becomes more significant, and therefore we present only the simulation results in Fig. 8(c). As observed before, an important piece of information from Fig. 8(c) is that Poisson white noise may effect asymmetries of the mean TPS with respect to the forward versus the backward transition.

The effect of U and I_0 on the $\tau_{shape}^{TP}(y|x_A)$ and $\tau_{shape}^{TP}(y|x_B)$ as revealed in Fig. 9. With the increase of U or I_0 , both $\tau_{shape}^{TP}(y|x_A)$ and $\tau_{shape}^{TP}(y|x_B)$ decrease gradually.

4.2. Transition path time

4.2.1. Linear potential

To study the mean TPT for the stochastic process (1) driven by Poisson white noise we first consider the case of the linear potential function shown in Fig. 1. Approximate theoretical expressions for the mean TPT for the forward and backward directions were obtained in Eqs. (30) and (37). Accordingly we obtain the follow-

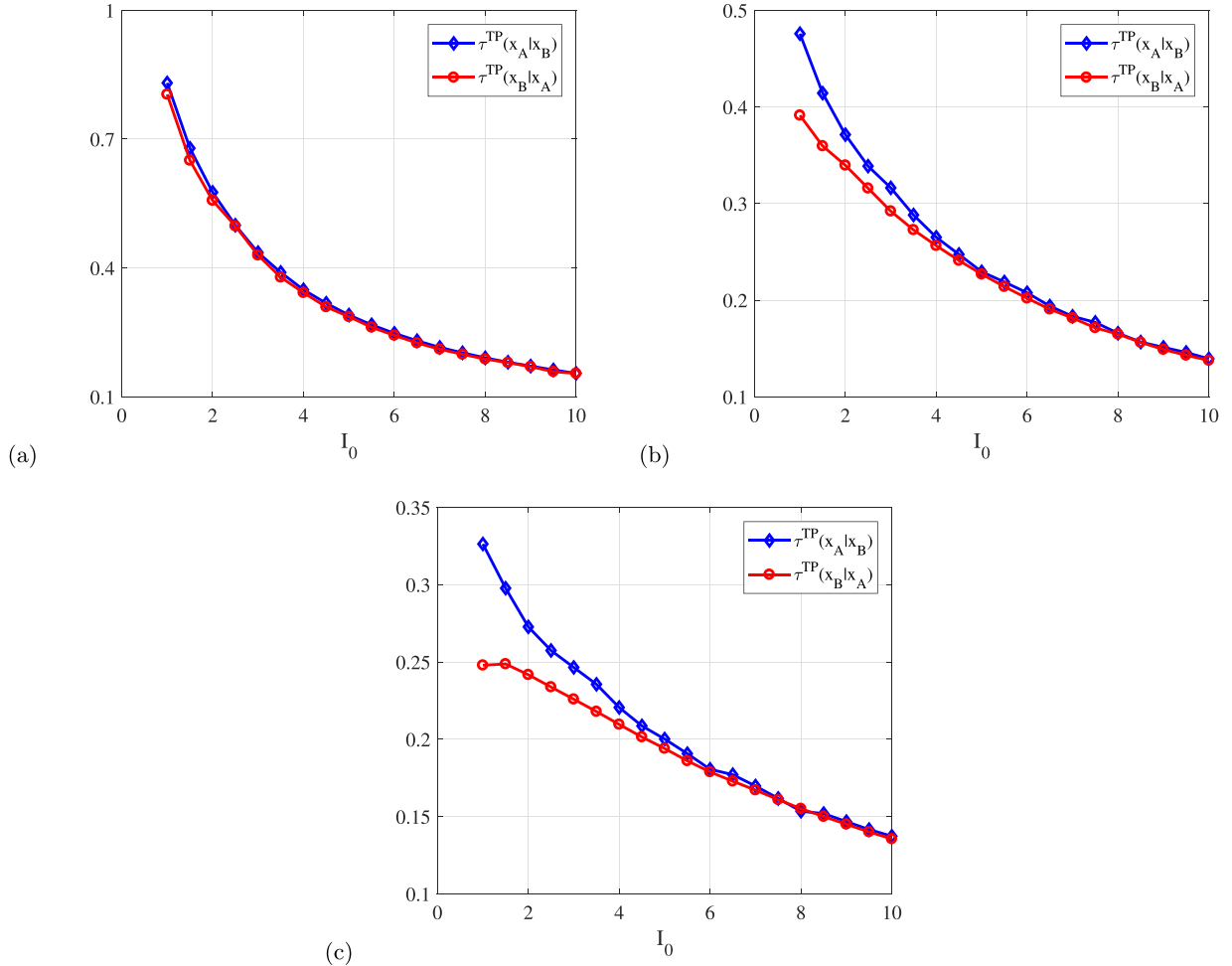


Fig. 13. Comparison of the mean TPT for transition paths from x_B to x_A with those in the opposite direction from x_A to x_B , for $E[Y^2] = 10^{-2}$ and $I_0 \in [1, 10]$, based on the results shown in Fig. 9. The respective barrier height are (a) $U = 3$, (b) $U = 8$, and (c) $U = 15$.

ing forms

$$M_{11}(x_B) = \frac{2}{cl_0} \left[\frac{2I_0}{U} \left(1 - \frac{I_0}{U} \right) e^{\frac{U}{l_0}} + \frac{2I_0}{U} \left(1 + \frac{I_0}{U} \right) e^{-\frac{U}{l_0}} \right], \quad (39a)$$

$$\bar{M}_{11}(x_A) = \frac{2}{cl_0} \left[\frac{2I_0}{U} \left(1 - \frac{I_0}{U} \right) e^{\frac{U}{l_0}} + \frac{2I_0}{U} \left(\frac{I_0}{U} + 1 \right) e^{-\frac{U}{l_0}} \right], \quad (39b)$$

the remaining terms are derived in Appendix B. Obviously, both terms are equal and have a similar dependence on the barrier height U as the respective terms (38) for the mean TPS. The numerical results of the mean TPT for these three potential functions are also obtained by the FFS scheme.

Fig. 10 exhibits the mean TPT of transition paths with different heights of the potential, as derived from Eqs. (30) and (37). Fig. 10(a) shows the mean TPT of transition paths from x_B to x_A as function of the noise intensity I_0 . We see that the mean TPT decreases with increasing noise intensity I_0 , as it should. Moreover, the mean TPT has an increasing trend with decreasing potential height U , albeit this difference becomes hardly distinguishable for large noise intensities. A similar behavior is observed in Fig. 10(b), which displays the mean TPT of transitions from x_A to x_B as function of the noise intensity I_0 . The behaviour is analogous to panel Fig. 10(a). With the increase of U , $\tau^{TP}(x_B|x_A)$ decreases gradually as presented in Fig. 10(c). U has a similar effect on $\tau^{TP}(x_A|x_B)$. In all cases the agreement with results from our theoretical approximation scheme is very good. The error $|\tau_{\text{theo}}^{TP} - \tau_{\text{sim}}^{TP}|$ between the theoretical and the simulation results is indicated in Fig. 10(d), where

$|\cdot|$ denotes the absolute value. As can be seen the error increases approximately linearly with the perturbation parameter ε .

As $M_{11}(x_B) = \bar{M}_{11}(x_A)$ according to Eq. (39), it is the term containing the perturbation parameter ε that controls how much $\tau^{TP}(x_B|x_A)$ and $\tau^{TP}(x_A|x_B)$ differ from each other. Indeed, we can see from Eqs. (30) and (37) that when the perturbation parameter ε becomes large, the mean TPT $\tau^{TP}(x_B|x_A)$ becomes increasingly disparate from $\tau^{TP}(x_A|x_B)$. However, when ε is relatively large, our approximate theoretical results are no longer accurate. Therefore, we numerically compare the mean TPT in the two directions with variation of the barrier height when the noise intensity is relatively small, that is, the corresponding perturbation parameter ε is relatively large. The results are presented in Fig. 11. Indeed, as the noise intensity I_0 decreases, the mean TPT in the two directions is no longer equal. Similarly, it can be observed that as the barrier height U increases, the disparity between the mean TPT in the two directions becomes more prominent. We conclude that for the linear potential function, the noise intensity of the Poisson white noise and the barrier height can influence the degree of deviation of the mean TPT in the two directions.

4.2.2. Harmonic ramp

We now turn to the mean TPT behavior for the harmonic ramp potential driven by Poisson white noise. For this case we exhibit the curves based on Eqs. (30) and (37) for the two directions of the transition paths in Fig. 12. As before, the mean TPT decreases with increasing noise strength I_0 and with decreasing bar-

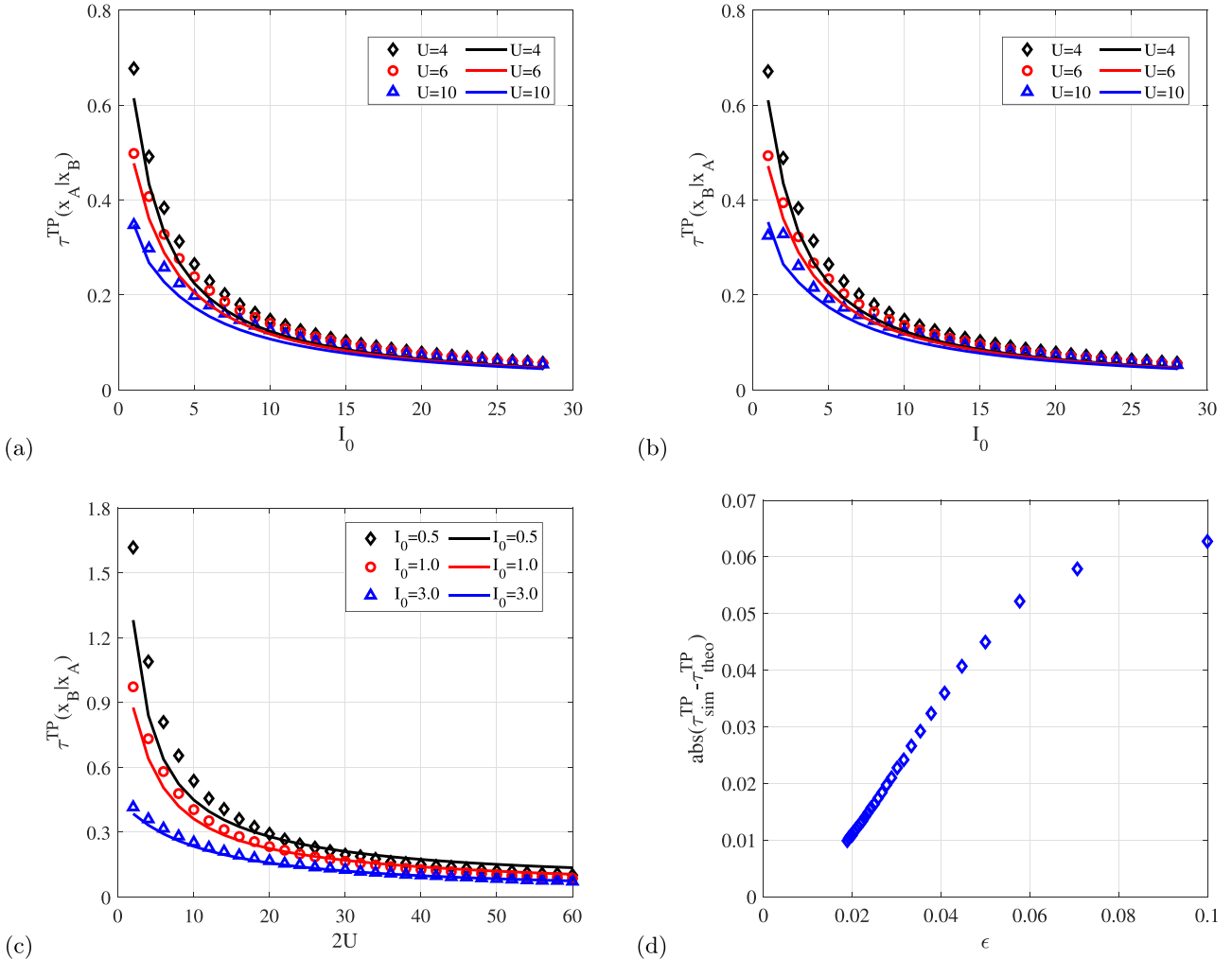


Fig. 14. (a) Mean TPT $\tau^{\text{TP}}(x_B|x_A)$ for transition paths from x_B to x_A , where $I_0 \in [1, 28]$ and $\mathbb{E}[Y^2] = 10^{-2}$; (b) Mean TPT $\tau^{\text{TP}}(x_B|x_A)$ for transitions in the opposite direction from x_A to x_B , where $I_0 \in [1, 28]$ and $\mathbb{E}[Y^2] = 10^{-2}$; (c) $\tau^{\text{TP}}(x_B|x_A)$ changes with U , where $U \in [1, 30]$ and $\mathbb{E}[Y^2] = 10^{-3}$. In both panels (a), (b) and (c) symbols represent results from the numerical FFS scheme while the lines represent our theoretical results based on Eqs. (30) and (37). (d) Absolute deviation between the theoretical and numerical results for the mean TPT.

rier height U for paths from x_B to x_A in panel 12(a), the analogous trend for the opposite direction is shown in panel Fig. 12(b). For ease of observation, in Fig. 12(c), only the change of $\tau^{\text{TP}}(x_B|x_A)$ with U is considered. It is clear that a small U leads to a larger $\tau^{\text{TP}}(x_B|x_A)$. Comparing the theoretical and numerical results in Figs. 12(a), 12(b) and 12(c) we see that our approximate theoretical results show very good agreement over the entire parameter range. In Fig. 12(d) we analyze the absolute deviation $|\tau_{\text{theo}}^{\text{TP}} - \tau_{\text{sim}}^{\text{TP}}|$ between the theoretical and the numerical results. We observe an almost linear increase of the deviation with growing perturbation parameter ϵ .

Fig. 13 shows the effects of noise intensity and barrier height on the mean TPT in both directions of the transition paths. As before, this comparison is based on numerical results, as for large perturbation parameter ϵ our approximate scheme becomes less reliable. Similar to the linear potential case the discrepancy between the two directions for small noise intensity I_0 and high barrier height U is obvious. Again, this discrepancy is due to the employed Poisson white noise, in contrast to the case of Gaussian white noise.

4.2.3. Inverted parabolic potential

We finally consider the case of an inverted parabolic potential centered around its maximum at the origin. As we can see in

Fig. 14 the general behavior is in line with the previous results for the linear potential and the harmonic ramp.

Fig. 15 shows a somewhat surprising result in comparison to our previous analysis. Namely, when we compare the mean TPT in the two directions of transition paths for different barrier heights U as function of the noise intensity I_0 , the agreement between both is almost perfect in all cases. We conclude that for this potential type the symmetry is more robust in the analyzed parameter range, even in the presence of Poisson white noise.

5. Conclusions

We developed an approximation scheme for the mean TPS and the mean TPT of transitions paths across different barrier shapes for a stochastic process driven by Poisson white noise. In particular we obtained an asymptotic expression for the mean TPS and the mean TPT in the linear potential case. Combining the approximative results with a numerical FFS scheme we analyzed in detail the influence of the different model parameters of the potential function and the Poisson white noise on the mean TPS and the mean TPT. We observe generally very good agreement between the theoretical approximation and the numerical results, over the entire range of parameters that we analyzed. Deviations between numerical results and the approximative scheme naturally emerge when

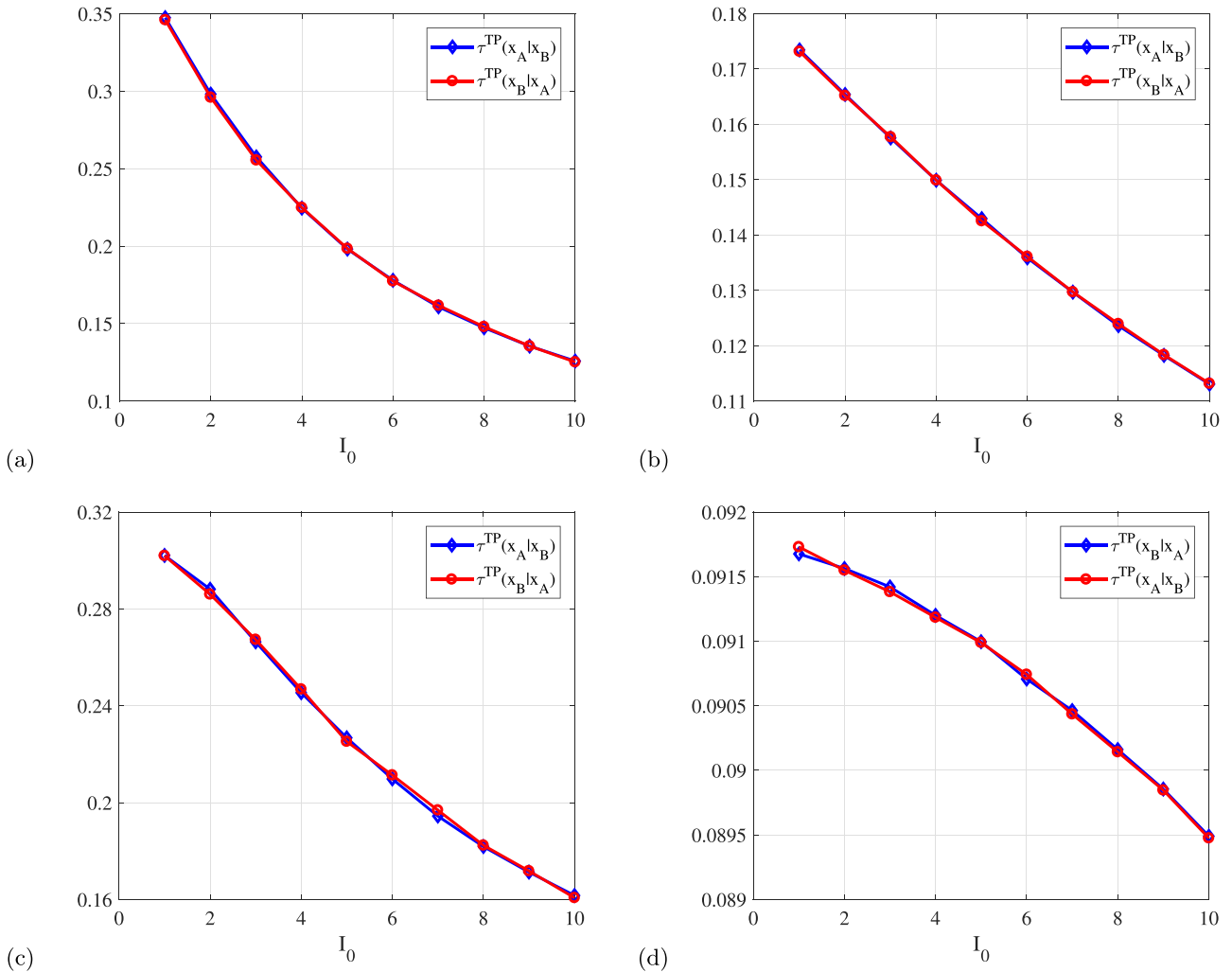


Fig. 15. Simulations results of the mean TPT for particle from x_B to x_A and x_A to x_B , $I_0 \in [1, 10]$. (a) $E[Y^2] = 10^{-2}$, $U = 10$; (b) $E[Y^2] = 10^{-2}$, $U = 30$; (c) $E[Y^2] = 0.1$, $U = 10$; (d) $E[Y^2] = 1$, $U = 30$.

the perturbation parameter assumes larger values, in particular, for low noise intensities and large barrier heights. This error can be decreased by taking along additional terms in our expansion. However, the detailed theoretical analysis of this point is considerably more involved and will therefore be performed in a future work.

A remarkable result is the observed asymmetry between the mean TPS and the mean TPT of the process with respect to the forward versus backward direction of the transition paths. While for Gaussian white noise the symmetry persists over the entire parameter range, in the case of Poisson white noise we demonstrated how the asymmetry grows with higher barriers and lower noise intensities. Interestingly, the asymmetry was shown to also depend on the precise barrier shape: for the inverted parabolic potential the asymmetry turned out to be much reduced in the analyzed parameter range in comparison to the linear potential and the harmonic ramp. As for many realistic systems the assumption of Gaussian white noise as the nature of the driving stochastic force is not justified, this point will certainly deserve further study in the future.

Apart from Poisson white noise, it will be of interest to study the mean TPS and the mean TPT for other types of noise, in particular, for Lévy white noise. Indeed, for Lévy motion the first-passage and first-hitting dynamics is strikingly different from the case of Gaussian noise [48–50], such that we would expect interesting effects for the transition path dynamics, as well.

Declaration of Competing Interest

The authors declare that they have no known competing financial interests or personal relationships that could have appeared to influence the work reported in this paper.

CRediT authorship contribution statement

Hua Li: Conceptualization, Methodology, Software, Formal analysis, Writing - original draft. **Yong Xu:** Conceptualization, Writing - original draft. **Ralf Metzler:** Writing - review and editing. **Jürgen Kurths:** Writing - review and editing.

Acknowledgments

This paper was supported by the National Natural Science Foundation of China under Grant No. 11772255, the Fundamental Research Funds for the Central Universities, the Research Funds for Interdisciplinary Subject of Northwestern Polytechnical University, the Shaanxi Project for Distinguished Young Scholars, and Shaanxi Provincial Key R&D Program 2020KW-013 and 2019TD-010. RM acknowledges support from German Science Foundation (DFG, project ME 1535/7-1) and the Foundation for Polish Science (Fundacja na rzecz Nauki Polskiej, FNP) within an Alexander von Humboldt Polish Honorary Research Scholarship.

Appendix A. Detailed theoretical results of the mean transition path shape of linear potential

A1. Mean transition path shape $\tau_{\text{shape}}^{\text{TP}}(y|x_A)$ of particle from x_A to y

For the linear case, $V(x) = \frac{U(x-1)}{2}$, one can easily obtain

$$\phi_{A_0}(y) = \frac{\alpha I_0}{U} \left[1 - e^{\frac{U}{I_0}(y-1)} \right], \quad (\text{A1})$$

$$\text{where } \alpha^{-1} = \frac{I_0}{U} \left(1 - e^{-\frac{2U}{I_0}} \right).$$

Then, the $K_0^{(1)}(x_A|y)$ has the following form:

$$\begin{aligned} K_0^{(1)}(x_A|y) &= \phi_{A_0}(y) \int_{x_A}^y \int_x^{x_B} \frac{2}{I_0} \phi_{A_0}(s) e^{-\frac{2}{I_0}V(s)} ds e^{\frac{2}{I_0}V(x)} dx - \phi_{B_0}(y) \int_y^{x_B} \int_x^{x_B} \frac{2}{I_0} \phi_{A_0}(s) e^{-\frac{2}{I_0}V(s)} ds e^{\frac{2}{I_0}V(x)} dx \\ &= \phi_{A_0}(y) \frac{2}{c I_0} \left[\frac{I_0}{U} e^{\frac{U}{I_0}(y-1)} - \frac{I_0}{U} \left(1 + \frac{2I_0}{U} \right) e^{\frac{U}{I_0}y} + \frac{2I_0}{U} \left(1 + \frac{I_0}{U} \right) e^{-\frac{U}{I_0}} + \frac{I_0}{U} y e^{\frac{U}{I_0}y} \right] \\ &\quad - \phi_{B_0}(y) \frac{2}{c I_0} \left[\frac{I_0}{U} \left(1 - \frac{2I_0}{U} \right) e^{\frac{U}{I_0}} - \frac{I_0}{U} y e^{\frac{U}{I_0}} + \frac{I_0}{U} \left(1 + \frac{2I_0}{U} \right) e^{\frac{U}{I_0}y} - \frac{I_0}{U} y e^{\frac{U}{I_0}y} \right], \end{aligned} \quad (\text{A2})$$

$$\text{where } c = e^{\frac{U}{I_0}} - e^{-\frac{U}{I_0}}, M_{12}(y) = \frac{2}{c I_0} \left[\frac{I_0}{U} \left(1 - \frac{2I_0}{U} \right) e^{\frac{U}{I_0}} - \frac{I_0}{U} y e^{\frac{U}{I_0}} + \frac{I_0}{U} \left(1 + \frac{2I_0}{U} \right) e^{\frac{U}{I_0}y} - \frac{I_0}{U} y e^{\frac{U}{I_0}y} \right].$$

Meanwhile,

$$\begin{aligned} M_{21_1}(y) &= \int_{x_A}^y \int_x^{x_B} \frac{2}{I_0} G_{11}(s) e^{-\frac{2}{I_0}V(s)} ds e^{\frac{2}{I_0}V(x)} dx \\ &= \frac{I_2}{12I_0} \left(\frac{4\alpha U}{I_0^2} - \frac{\alpha \alpha_1 U^3}{I_0^3} \right) \left[\frac{I_0}{U} \left(1 + \frac{I_0}{U} \right) e^{\frac{U}{I_0}(y-1)} - \frac{I_0}{U} \left(2 + \frac{I_0}{U} \right) e^{-\frac{2U}{I_0}} - \frac{I_0}{U} y e^{\frac{U}{I_0}(y-1)} \right] \\ &\quad + \frac{I_2 U^3}{6c I_0^5} \left[\left(\frac{I_0^3}{U^3} + \frac{2I_0^2}{U^2} + \frac{2I_0}{U} \right) e^{-\frac{U}{I_0}} - \left(\frac{I_0^3}{U^3} + \frac{I_0^2}{U^2} + \frac{I_0}{2U} \right) e^{\frac{U}{I_0}y} + \frac{I_0}{U} \left(1 + \frac{I_0}{U} \right) y e^{\frac{U}{I_0}y} - \frac{I_0}{2U} y^2 e^{\frac{U}{I_0}y} \right], \end{aligned} \quad (\text{A3})$$

$$\begin{aligned} M_{21_2}(y) &= \int_{x_A}^y \int_x^{x_B} \frac{2}{I_0} G_{12}(s) e^{-\frac{2}{I_0}V(s)} ds e^{\frac{2}{I_0}V(x)} dx \\ &= \frac{\alpha I_2 U^2}{6c I_0^4} \left[\left(2 + \frac{I_0}{U} \right) e^{-\frac{2U}{I_0}} - \frac{I_0}{U} \right] \left[\frac{I_0}{U} e^{\frac{U}{I_0}(y-1)} - \frac{I_0}{U} \left(1 + \frac{2I_0}{U} \right) e^{\frac{U}{I_0}y} + \frac{2I_0}{U} \left(1 + \frac{I_0}{U} \right) e^{-\frac{U}{I_0}} + \frac{I_0}{U} y e^{\frac{U}{I_0}y} \right] \\ &\quad + \frac{\alpha I_2 U^2}{6I_0^4} \left[\begin{array}{l} \frac{I_0}{U} \left(\frac{3I_0^2}{U^2} + \frac{4I_0}{U} + 2 \right) e^{-\frac{2U}{I_0}} - \frac{I_0}{U} \left(\frac{3I_0^2}{U^2} + \frac{2I_0}{U} + \frac{1}{2} \right) e^{\frac{U}{I_0}(y-1)} \\ + \frac{I_0}{U} \left(1 + \frac{2I_0}{U} \right) y e^{\frac{U}{I_0}(y-1)} - \frac{I_0}{2U} y^2 e^{\frac{U}{I_0}(y-1)} + \frac{I_0^2}{U^2} (y+1) \end{array} \right], \end{aligned} \quad (\text{A4})$$

$$\text{where } \alpha_1 = \frac{2}{I_0} \left[\frac{2I_0}{U} \left(1 - \frac{I_0}{U} \right) e^{\frac{U}{I_0}} + \frac{2I_0}{U} \left(1 + \frac{I_0}{U} \right) e^{-\frac{U}{I_0}} \right] / c, \text{ and}$$

$$\begin{aligned} M_{22_1}(y) &= \int_y^{x_B} \int_x^{x_B} \frac{2}{I_0} G_{11}(s) e^{-\frac{2}{I_0}V(s)} ds e^{\frac{2}{I_0}V(x)} dx \\ &= \frac{I_2}{12I_0} \left(\frac{4\alpha U}{I_0^2} - \frac{\alpha \alpha_1 U^3}{I_0^3} \right) \left[\frac{I_0}{U} y e^{\frac{U}{I_0}(y-1)} - \frac{I_0}{U} \left(1 + \frac{I_0}{U} \right) e^{\frac{U}{I_0}(y-1)} + \frac{I_0^2}{U^2} \right] \\ &\quad + \frac{I_2 U^3}{6c I_0^5} \left[-\frac{I_0^3}{U^3} e^{\frac{U}{I_0}} + \frac{I_0}{U} \left(\frac{I_0^2}{U^2} + \frac{I_0}{U} + \frac{1}{2} \right) e^{\frac{U}{I_0}y} - \frac{I_0}{U} \left(1 + \frac{I_0}{U} \right) y e^{\frac{U}{I_0}y} + \frac{I_0}{2U} y^2 e^{\frac{U}{I_0}y} \right], \end{aligned} \quad (\text{A5})$$

$$\begin{aligned} M_{22_2}(y) &= \int_y^{x_B} \int_x^{x_B} \frac{2}{I_0} G_{12}(s) e^{-\frac{2}{I_0}V(s)} ds e^{\frac{2}{I_0}V(x)} dx \\ &= \frac{\alpha I_2 U^2}{6c I_0^4} \left[\left(\frac{I_0}{U} + 2 \right) e^{-\frac{2U}{I_0}} - \frac{I_0}{U} \right] \left[\frac{I_0}{U} \left(1 - \frac{2I_0}{U} \right) e^{\frac{U}{I_0}} - \frac{I_0}{U} e^{\frac{U}{I_0}} y + \frac{I_0}{U} \left(1 + \frac{2I_0}{U} \right) e^{\frac{U}{I_0}y} - \frac{I_0}{U} y e^{\frac{U}{I_0}y} \right] \\ &\quad + \frac{\alpha I_2 U^2}{6I_0^4} \left[\begin{array}{l} \frac{I_0}{U} y^2 e^{\frac{U}{I_0}(y-1)} - \frac{I_0}{U} \left(1 + \frac{2I_0}{U} \right) y e^{\frac{U}{I_0}(y-1)} - \frac{I_0^2}{U^2} y \\ + \frac{I_0}{U} \left(\frac{3I_0^2}{U^2} + \frac{2I_0}{U} + \frac{1}{2} \right) e^{\frac{U}{I_0}(y-1)} + \frac{I_0^2}{U^2} \left(1 - \frac{3I_0}{U} \right) \end{array} \right]. \end{aligned} \quad (\text{A6})$$

According to Eq. (22), one has

$$\phi_{A_2}(y) = \frac{I_2 \alpha U^2}{12I_0^3} \left\{ \left[\left(2 + \frac{I_0}{U} \right) e^{-\frac{2U}{I_0}} - \frac{I_0}{U} \right] \phi_{A_0}(y) - \left(1 + \frac{I_0}{U} \right) e^{\frac{2}{I_0}V(y)} + y e^{\frac{2}{I_0}V(y)} + \frac{I_0}{U} \right\}, \quad (\text{A7})$$

$$\text{where } G_{11}(y) = \frac{I_2}{24} K_0^{(1)(4)}(x_A|y), G_{12}(y) = \phi_{A_2}(y), M_{21}(y) = M_{21_1}(y) + M_{21_2}(y), M_{22}(y) = M_{22_1}(y) + M_{22_2}(y).$$

A2. Mean TPS $\tau_{\text{shape}}^{\text{TP}}(y|x_B)$ of particle from x_B to y

For the particle in the linear potential from x_B to y , we get

$$\phi_{B_0}(y) = \frac{\alpha I_0}{U} \left[e^{\frac{U}{I_0}(y-1)} - e^{-\frac{2U}{I_0}} \right]. \quad (\text{A8})$$

Then, the $K_0^{(1)}(x_B|y)$ could be derived from Eq. (34)

$$\begin{aligned} K_0^{(1)}(x_B|y) &= \phi_{B_0}(y) \int_y^{x_B} \int_{x_A}^x \frac{2}{I_0} \phi_{B_0}(s) e^{-\frac{2}{I_0}V(s)} ds e^{\frac{2}{I_0}V(x)} dx - \phi_{A_0}(y) \int_{x_A}^y \int_{x_A}^x \frac{2}{I_0} \phi_{B_0}(s) e^{-\frac{2}{I_0}V(s)} ds e^{\frac{2}{I_0}V(x)} dx \\ &= \phi_{B_0}(y) \frac{2}{cI_0} \left[\frac{2I_0}{U} \left(1 - \frac{I_0}{U} \right) e^{\frac{U}{I_0}} + \frac{I_0}{U} \left(\frac{2I_0}{U} - 1 \right) e^{\frac{U}{I_0}y} - \frac{I_0}{U} y e^{\frac{U}{I_0}y} + \frac{I_0}{U} e^{-\frac{U}{I_0}} (1-y) \right] \\ &\quad - \phi_{A_0}(y) \frac{2}{cI_0} \left[\frac{I_0}{U} \left(1 + \frac{2I_0}{U} \right) e^{-\frac{U}{I_0}} + \frac{I_0}{U} \left(1 - \frac{2I_0}{U} \right) e^{\frac{U}{I_0}y} + \frac{I_0}{U} y e^{\frac{U}{I_0}y} + \frac{I_0}{U} e^{-\frac{U}{I_0}y} \right], \end{aligned} \quad (\text{A9})$$

$$\text{where } \bar{M}_{12}(y) = \frac{2}{cI_0} \left[\frac{I_0}{U} \left(1 + \frac{2I_0}{U} \right) e^{-\frac{U}{I_0}} + \frac{I_0}{U} \left(1 - \frac{2I_0}{U} \right) e^{\frac{U}{I_0}y} + \frac{I_0}{U} y e^{\frac{U}{I_0}y} + \frac{I_0}{U} e^{-\frac{U}{I_0}y} \right].$$

Moreover,

$$\begin{aligned} \bar{M}_{21_1}(y) &= \int_y^{x_B} \int_{x_A}^x \frac{2}{I_0} G_{21}(s) e^{-\frac{2}{I_0}V(s)} ds e^{\frac{2}{I_0}V(x)} dx \\ &= \frac{I_2}{12I_0} \left(\frac{\alpha\alpha_1 U^3}{I_0^3} - \frac{4\alpha U}{I_0^2} \right) \left[\frac{I_0}{U} \left(2 - \frac{I_0}{U} \right) + \frac{I_0}{U} \left(\frac{I_0}{U} - 1 \right) e^{\frac{U}{I_0}(y-1)} - \frac{I_0}{U} y e^{\frac{U}{I_0}(y-1)} \right] \\ &\quad - \frac{I_2 U^3}{6cI_0^5} \left[\frac{I_0}{U} \left(\frac{I_0^2}{U^2} - \frac{2I_0}{U} + 2 \right) e^{\frac{U}{I_0}} - \frac{I_0}{U} \left(\frac{I_0^2}{U^2} - \frac{I_0}{U} + \frac{1}{2} \right) e^{\frac{U}{I_0}y} + \frac{I_0}{U} \left(\frac{I_0}{U} - 1 \right) y e^{\frac{U}{I_0}y} - \frac{I_0}{2U} y^2 e^{\frac{U}{I_0}y} \right], \end{aligned} \quad (\text{A10})$$

$$\begin{aligned} \bar{M}_{21_2}(y) &= \int_y^{x_B} \int_{x_A}^x \frac{2}{I_0} G_{22}(s) e^{-\frac{2}{I_0}V(s)} ds e^{\frac{2}{I_0}V(x)} dx \\ &= \frac{\alpha I_2 U^2}{6cI_0^4} \left[\left(2 - \frac{I_0}{U} \right) + \frac{I_0}{U} e^{-\frac{2U}{I_0}} \right] \left[\frac{2I_0}{U} \left(1 - \frac{I_0}{U} \right) e^{\frac{U}{I_0}} - \frac{I_0}{U} \left(1 - \frac{2I_0}{U} \right) e^{\frac{U}{I_0}y} - \frac{I_0}{U} y e^{\frac{U}{I_0}y} + \frac{I_0}{U} e^{-\frac{U}{I_0}} (1-y) \right] \\ &\quad - \frac{\alpha I_2 U^2}{6I_0^4} \left[\begin{array}{l} \frac{I_0}{U} \left(\frac{2I_0^2}{U^2} - \frac{3I_0}{U} + 2 \right) - \frac{I_0}{U} \left(\frac{2I_0^2}{U^2} - \frac{I_0}{U} + \frac{1}{2} \right) e^{\frac{U}{I_0}(y-1)} \\ + \frac{I_0}{U} \left(\frac{2I_0}{U} - 1 \right) y e^{\frac{U}{I_0}(y-1)} - \frac{I_0}{2U} y^2 e^{\frac{U}{I_0}(y-1)} + \frac{I_0}{U} (y-1) e^{-\frac{2U}{I_0}} \end{array} \right], \end{aligned} \quad (\text{A11})$$

and

$$\begin{aligned} \bar{M}_{22_1}(y) &= \int_{x_A}^y \int_{x_A}^x \frac{2}{I_0} G_{21}(s) e^{-\frac{2}{I_0}V(s)} ds e^{\frac{2}{I_0}V(x)} dx \\ &= \frac{I_2}{12I_0} \left(\frac{\alpha\alpha_1 U^3}{I_0^3} - \frac{4\alpha U}{I_0^2} \right) \left[\frac{I_0^2}{U^2} e^{-\frac{2U}{I_0}} - \frac{I_0}{U} \left(\frac{I_0}{U} - 1 \right) e^{\frac{U}{I_0}(y-1)} + \frac{I_0}{U} y e^{\frac{U}{I_0}(y-1)} \right] \\ &\quad - \frac{I_2 U^3}{6cI_0^5} \left[-\frac{I_0^3}{U^3} e^{-\frac{U}{I_0}} + \frac{I_0}{U} \left(\frac{I_0^2}{U^2} - \frac{I_0}{U} + \frac{1}{2} \right) e^{\frac{U}{I_0}y} + \frac{I_0}{U} \left(1 - \frac{I_0}{U} \right) y e^{\frac{U}{I_0}y} + \frac{I_0}{2U} y^2 e^{\frac{U}{I_0}y} \right], \end{aligned} \quad (\text{A12})$$

$$\begin{aligned} \bar{M}_{22_2}(y) &= \int_{x_A}^y \int_{x_A}^x \frac{2}{I_0} G_{22}(s) e^{-\frac{2}{I_0}V(s)} ds e^{\frac{2}{I_0}V(x)} dx \\ &= \frac{\alpha I_2 U^2}{6cI_0^4} \left[\left(2 - \frac{I_0}{U} \right) + \frac{I_0}{U} e^{-\frac{2U}{I_0}} \right] \left[\frac{I_0}{U} \left(\frac{2I_0}{U} + 1 \right) e^{-\frac{U}{I_0}} + \frac{I_0}{U} \left(1 - \frac{2I_0}{U} \right) e^{\frac{U}{I_0}y} + \frac{I_0}{U} y e^{\frac{U}{I_0}y} + \frac{I_0}{U} e^{-\frac{U}{I_0}y} \right] \\ &\quad - \frac{\alpha I_2 U^2}{6I_0^4} \left[\begin{array}{l} -\frac{I_0}{U} \left(\frac{2I_0^2}{U^2} + \frac{I_0}{U} + 1 \right) e^{-\frac{2U}{I_0}} + \frac{I_0}{U} \left(\frac{2I_0^2}{U^2} - \frac{I_0}{U} + \frac{1}{2} \right) e^{\frac{U}{I_0}(y-1)} \\ + \frac{I_0}{U} \left(1 - \frac{2I_0}{U} \right) y e^{\frac{U}{I_0}(y-1)} + \frac{I_0}{2U} y^2 e^{\frac{U}{I_0}(y-1)} - \frac{I_0}{U} y e^{-\frac{2U}{I_0}} \end{array} \right]. \end{aligned} \quad (\text{A13})$$

Then,

$$\phi_{B_2}(y) = \frac{I_2 \alpha U^2}{12I_0^3} \left\{ \left[\left(2 - \frac{I_0}{U} \right) + \frac{I_0}{U} e^{-\frac{2U}{I_0}} \right] \phi_{B_0}(y) - \left(1 - \frac{I_0}{U} \right) e^{\frac{2}{I_0}V(y)} - y e^{\frac{2}{I_0}V(y)} - \frac{I_0}{U} e^{-\frac{2U}{I_0}} \right\}, \quad (\text{A14})$$

where $G_{21}(y) = \frac{I_2}{24} K_0^{(1)(4)}(x_B|y)$, $G_{22}(y) = \phi_{B_2}(y)$, $\bar{M}_{21}(y) = \bar{M}_{21_1}(y) + \bar{M}_{21_2}(y)$, $\bar{M}_{22}(y) = \bar{M}_{22_1}(y) + \bar{M}_{22_2}(y)$.

Appendix B. Detailed theoretical results of the mean transition path time of linear potential

B1. Mean TPT $\tau^{\text{TPT}}(x_A|x_B)$ of particle from x_B to x_A

The main term of the mean TPT as shown in the Eq. (39) of a particle in the linear potential function from x_B to x_A is

$$M_{11}(x_B) = \frac{2}{cI_0} \left[\frac{2I_0}{U} \left(1 - \frac{I_0}{U} \right) e^{\frac{U}{I_0}} + \frac{2I_0}{U} \left(1 + \frac{I_0}{U} \right) e^{-\frac{U}{I_0}} \right]. \quad (\text{B1})$$

According to the Eq. (27)

$$\begin{aligned} M_{21_1}(x_B) &= \int_{x_A}^{x_B} \int_x^{x_B} \frac{2}{I_0} G_{11}(s) e^{-\frac{2}{l_0} V(s)} dse^{\frac{2}{l_0} V(x)} dx \\ &= \frac{I_2}{12l_0} \left(\frac{4\alpha U}{l_0^2} - \frac{\alpha\alpha_1 U^3}{l_0^3} \right) \left[\frac{l_0^2}{U^2} - \frac{l_0}{U} \left(2 + \frac{l_0}{U} \right) e^{-\frac{2U}{l_0}} \right] \\ &\quad + \frac{I_2 U^3}{6cl_0^5} \left[\frac{l_0}{U} \left(\frac{l_0^2}{U^2} + \frac{2l_0}{U} + 2 \right) e^{-\frac{U}{l_0}} - \frac{l_0^3}{U^3} e^{\frac{U}{l_0}} \right], \end{aligned} \quad (\text{B2})$$

$$\begin{aligned} M_{21_2}(x_B) &= \int_{x_A}^{x_B} \int_x^{x_B} \frac{2}{I_0} G_{12}(s) e^{-\frac{2}{l_0} V(s)} dse^{\frac{2}{l_0} V(x)} dx \\ &= \frac{\alpha I_2 U^2}{6cl_0^4} \left[\left(\frac{l_0}{U} + 2 \right) e^{-\frac{2U}{l_0}} - \frac{l_0}{U} \right] \left[\frac{2l_0}{U} \left(1 - \frac{l_0}{U} \right) e^{\frac{U}{l_0}} + \frac{2l_0}{U} \left(1 + \frac{l_0}{U} \right) e^{-\frac{U}{l_0}} \right] \\ &\quad + \frac{\alpha I_2 U^2}{6l_0^4} \left[\frac{l_0}{U} \left(\frac{3l_0^2}{U^2} + \frac{4l_0}{U} + 2 \right) e^{-\frac{2U}{l_0}} + \frac{l_0^2}{U^2} \left(2 - \frac{3l_0}{U} \right) \right]. \end{aligned} \quad (\text{B3})$$

And in the Eq. (22)

$$\begin{aligned} N_1(y) &= \int_{x_A}^y \int_x^{x_B} \frac{2}{I_0} g_1(s) e^{-\frac{2}{l_0} V(s)} dse^{\frac{2}{l_0} V(x)} dx \\ &= \frac{\alpha I_2 U^2}{12l_0^3} \left[ye^{\frac{U}{l_0}(y-1)} - \left(1 + \frac{l_0}{U} \right) e^{\frac{U}{l_0}(y-1)} + \left(2 + \frac{l_0}{U} \right) e^{-\frac{2U}{l_0}} \right], \end{aligned} \quad (\text{B4})$$

we could obtain

$$N_1(x_B) = \frac{\alpha I_2 U^2}{12l_0^3} \left[\left(2 + \frac{l_0}{U} \right) e^{-\frac{2U}{l_0}} - \frac{l_0}{U} \right]. \quad (\text{B5})$$

B2. Mean TPT $\tau^{TP}(x_B|x_A)$ of particle from x_A to x_B

The main term of the mean TPT as shown in the Eq. (34) of a particle in the linear potential function from x_A to x_B is

$$\bar{M}_{11}(x_A) = \frac{2}{cl_0} \left[\frac{2l_0}{U} \left(1 - \frac{l_0}{U} \right) e^{\frac{U}{l_0}} + \frac{2l_0}{U} \left(\frac{l_0}{U} + 1 \right) e^{-\frac{U}{l_0}} \right]. \quad (\text{B6})$$

We can also get some terms as presented in Eq. (34)

$$\begin{aligned} \bar{M}_{21_1}(x_A) &= \int_{x_A}^{x_B} \int_{x_A}^x \frac{2}{I_0} G_{21}(s) e^{-\frac{2}{l_0} V(s)} dse^{\frac{2}{l_0} V(x)} dx \\ &= \frac{I_2}{12l_0} \left(\frac{\alpha\alpha_1 U^3}{l_0^3} - \frac{4\alpha U}{l_0^2} \right) \left[\frac{l_0}{U} \left(2 - \frac{l_0}{U} \right) + \frac{l_0^2}{U^2} e^{-\frac{2U}{l_0}} \right] \\ &\quad - \frac{I_2 U^3}{6cl_0^5} \left[\frac{l_0}{U} \left(\frac{l_0^2}{U^2} - \frac{2l_0}{U} + 2 \right) e^{\frac{U}{l_0}} - \frac{l_0^3}{U^3} e^{-\frac{U}{l_0}} \right], \end{aligned} \quad (\text{B7})$$

$$\begin{aligned} \bar{M}_{21_2}(x_A) &= \int_{x_A}^{x_B} \int_{x_A}^x \frac{2}{I_0} G_{22}(s) e^{-\frac{2}{l_0} V(s)} dse^{\frac{2}{l_0} V(x)} dx \\ &= \frac{\alpha I_2 U^2}{6cl_0^4} \left[\left(2 - \frac{l_0}{U} \right) + \frac{l_0}{U} e^{-\frac{2U}{l_0}} \right] \left[\frac{2l_0}{U} \left(1 - \frac{l_0}{U} \right) e^{\frac{U}{l_0}} + \frac{2l_0}{U} \left(1 + \frac{l_0}{U} \right) e^{-\frac{U}{l_0}} \right] \\ &\quad - \frac{\alpha I_2 U^2}{6l_0^4} \left[\frac{l_0}{U} \left(\frac{2l_0^2}{U^2} - \frac{3l_0}{U} + 2 \right) - \frac{l_0}{U} \left(\frac{2l_0^2}{U^2} + \frac{l_0}{U} + 2 \right) e^{-\frac{2U}{l_0}} \right]. \end{aligned} \quad (\text{B8})$$

Meanwhile, according to Eq. (32b), we also need to calculate

$$\begin{aligned} \bar{N}_1(y) &= \int_y^{x_B} \int_{x_A}^x \frac{2}{I_0} g_2(s) e^{-\frac{2}{l_0} V(s)} dse^{\frac{2}{l_0} V(x)} dx \\ &= \frac{\alpha I_2 U^2}{12l_0^3} \left[2 - \frac{l_0}{U} - ye^{\frac{U}{l_0}(y-1)} + \left(\frac{l_0}{U} - 1 \right) e^{\frac{U}{l_0}(y-1)} \right], \end{aligned} \quad (\text{B9})$$

then

$$\bar{N}_1(x_A) = \frac{\alpha I_2 U^2}{12l_0^3} \left(2 - \frac{l_0}{U} + \frac{l_0}{U} e^{-\frac{2U}{l_0}} \right). \quad (\text{B10})$$

References

- [1] Bachelier L. Théorie de la spéculation. *Annales Scientifiques de l'École Normale Supérieure* 1900;3(21).
- [2] Cootner PH. The random character of stock market prices. Cambridge MA: MIT Press; 1967.
- [3] Smoluchowski MV. *Z Phys Chem* 1917;92(129).
- [4] Redner S. A guide to first passage processes. Cambridge: Cambridge University press; 2001.
- [5] Metzler R, Oshanin G, Redner S. First passage problems: recent advances. Singapore: World Scientific; 2014.
- [6] Hughes BD. Random walks and random environments, vol 1: random walks. Oxford, UK: Oxford University Press; 1995.
- [7] Bénichou O, Chevalier C, Klafter J, Meyer B, Voituriez R. *Nature Chem* 2010;2(472).
- [8] Condamin S, Bénichou O, Tejedor V, Voituriez R, Klafter J. *Nature* 2007;450(77).
- [9] Bressloff PC, Newby JM. *Rev Mod Phys* 2013;85(135).
- [10] Holcman D, Schuss Z. *J Phys A* 2017;50(1).
- [11] Godec A, Metzler R. *Phys Rev X* 2016;6(041037).
- [12] Godec A, Metzler R. *J Phys A* 2017;50(084001).
- [13] Hartich D, Godec A. *New J Phys* 2018;20(112002).
- [14] Li YG, Mei RX, Xu Y, Kurths J, Duan JQ, Metzler R. *New J Phys* 2020;22(053016).
- [15] Palyulin V, Metzler R. *J Stat Mech* 2012;2012(L03001).
- [16] Mei RX, Xu Y, Li YG, Kurths J. *Chaos Soliton Fract* 2020;135(109766).
- [17] Képés F. *J Mol Biol* 2004;340(957).
- [18] Kuhlman TE, Cox EC. *Mol Syst Biol* 2012;8(610).
- [19] Kolesov G, Wunderlich Z, Laikova ON, Gelfand MS, Mirny LA. *Proc Natl Acad Sci USA* 2007;104(13948).
- [20] Pulkkinen O, Metzler R. *Phys Rev Lett* 2013;110(198101).
- [21] Collins FC, Kimball GE. *J Colloid Sci* 1949;4(425).
- [22] Grebenkov D, Metzler R, Oshanin G. *Comm Chem* 2018;1(96).
- [23] Mei RX, Xu Y, Kurths J. *Phys Rev E* 2019;100(022114).
- [24] Holcman D, Schuss Z. *SIAM Rev* 2014;56(213).
- [25] Grebenkov DS, Metzler R, Oshanin G. *New J Phys* 2019;21(122001).
- [26] Arrhenius S. *Z Phys Chem (Leipzig)* 1889;4(216).
- [27] Pollak E, Talkner P. *Chaos* 2005;15(026116).
- [28] Eyring H. *J Chem Phys* 1935;3(107).
- [29] Garrett BC. *Theor Chem Acc* 2000;103(200).
- [30] Wigner E. *Trans Faraday Soc* 1938;34(29).
- [31] Petersson GA. *Theor Chem Acc* 1995;103(190).
- [32] Kramers HA. *Physica* 1940;7(284).
- [33] Hänggi P, Talkner P, Borkovec M. *Rev Mod Phys* 1990;62(251).
- [34] Chung HS, McHale K, Louis JM, Eaton WA. *Science* 2012;335(981).
- [35] Chung HS, Eaton WA. *Nature* 2013;502(685).
- [36] Chung HS, Piana-Agostinetti S, Shaw DE, Eaton WA. *Science* 2015;349(1504).
- [37] Neupane K, Foster DAN, Dee DR, Yu H, Wang F, Woodside MT. *Science* 2016;352(239).
- [38] Sturzenegger F, Zosel F, Holmstrom ED, Buholzer KJ, Makarov DE, Nettels D, Schuler B. *Nat Comm* 2018;9(4708).
- [39] Neupane K, Dustin BR, Yu H, Daniel ANF, Wang F, Woodside MT. *Phys Rev Lett* 2012;109(068102).
- [40] Cossio P, Hummer G, Szabo A. *J Chem Phys* 2018;148(123309).
- [41] Makarova DE. *J Chem Phys* 2015;143(194103).
- [42] Chandler D. *J Chem Phys* 1978;68(2959).
- [43] Dellago C, Bolhuis PG, Chandler D. *J Chem Phys* 1998;108(9236).
- [44] Lu JF, Nolen J. *Probab Theory Rel* 2015;161(195).
- [45] Hawk AT, Konda SSM, Makarov DE. *J Chem Phys* 2013;139(064101).
- [46] Dellago C, Bolhuis PG, Geissler PL. *Adv Chem Phys* 2002;123(1).
- [47] Bolhuis PG, Chandler D, Dellago C, Geissler PL. *Ann Rev Phys Chem* 2002;53(291).
- [48] Koren T, Lomholt MA, Chechkin AV, Klafter J, Metzler R. *Phys Rev Lett* 2007;99(160602).
- [49] Palyulin VV, Blackburn G, Lomholt MA, Watkins NW, Metzler R, Klages R, Chechkin AV. *New J Phys* 2019;21(103028).
- [50] Padash A, Chechkin AV, Dybiec B, Pavlyukevich I, Schokri B, Metzler R. *J Phys A-Math Theor* 2019;52(454004).
- [51] Bressloff PC, Lawley SD. *J Phys A-Math Theor* 2015;48(225001).
- [52] Li H, Xu Y, Yue XL, Kurths J. *Physica A* 2019;532(121764).
- [53] Pyo AGT, Hoffer NO, Neupane K, Woodside MT. *J Chem Phys* 2018;149(1115101).
- [54] Hoffer NO, Neupane K, Woodside MT. *P Natl Acad SCI USA* 2019;116(8125).
- [55] Chung HS, Eaton WA. *Curr Opin Struc Biol* 2018;48(30).
- [56] Sahin B. *Phys Rev E* 2018;97(062406).
- [57] Lubensky DK. *Biophys J* 1999;77(1824).
- [58] Chung HS, Gopich IV. *Phys Chem Chem Phys* 2014;16(18644).
- [59] Chung HS. *J Mol Biol* 2018;430(409).
- [60] Hummer G. *J Chem Phys* 2004;120(516).
- [61] Berezhkovskii AM, Dagdug L, Bezrukov SM. *J Phys Chem B* 2020;124(2305).
- [62] Berezhkovskii AM, Leonardo D, Bezrukov SM. *J Phys Chem B* 2017;121(5455).
- [63] Hoffer NO, Woodside MT. *Curr Opin Struc Biol* 2019;53(68).
- [64] Li H, Xu Y, Li YG, Metzler R. *Eur Phys J Plus* 2020;135(9):1–22.
- [65] Laleman M, Carlon E, Orland H. *J Chem Phys* 2017;147(214103).
- [66] Berezhkovskii AM, Hummer G, Bezrukov SM. *Phys Rev Lett* 2006;97(020601).
- [67] Gladrow J, Ribezzi CM, Ritort F, Keyser UF. *Nat Commun* 2019;10(55).
- [68] Kim WK, Netz RR. *J Chem Phys* 2015;143(224108).
- [69] Zhang XY, Xu Y, Liu Q, Kurths J. *SCI China Technol Sc* 2020;63.
- [70] Ma JZ, Xu Y, Li YG, Tian RL, J Ma S, Kurths J. *Appl Math Mech-Engl* 2020. doi:10.1007/s10483-020-2672-8.
- [71] Roberts JB. *J Sound Vib* 1965;2(375).
- [72] Wu Y, Zhu WQ. *Phys Rev E* 2008;77(041911).
- [73] Schafer B, Beck C, Aihara K, Withaut D, Timme M. *Nat Energy* 2018;3(119).
- [74] Lin YK, Cai GQ. Probabilistic structural dynamics: advance theory and applications. New York: McGraw-Hill Press; 1995.
- [75] Ma JZ, Xu Y, Xu W, Li YG, Kurths J. *SCI China Technol Sc* 2019;62(2144).
- [76] Ma JZ, Xu Y, Li YG, Tian RL, Chen GR, Kurths J. *Nonlinear Dynam* 2020;101:21–35.
- [77] Jia WT, Xu Y, Li DX. *Entropy* 2018;20(143).
- [78] Yue XL, Xu W, Xu Y, Sun JQ. *Probabilist Eng Mech* 2019;55(102).
- [79] Ze LM, Chen JB, Antonina P. *Commun Nonlinear Sci* 2020;80(104974).
- [80] Malthus TR. An essay on the principle of population. Parasitic Ventures Press; 1878.
- [81] May RM. *Nature* 1976;261(459).
- [82] Dieterich E, Soler JC, Crivellari MR, Seifert U, Ritort F. *Nat Phys* 2015;11(971).
- [83] Allen RJ, Warren PB, Wolde PRT. *Phys Rev Lett* 2005;532(018104).
- [84] Li H, Xu Y, Kurths J, Yue XL. *Eur Phys J B* 2019;92(76).
- [85] Risken H. The Fokker-Planck equation: method of solution and application. Berlin: Springer-Verlag; 1989.
- [86] Cai GQ, Lin YK. *Int J Nonlin Mech* 1991;27(955).
- [87] Xu Y, Li H, Wang HY, Jia WT, Yue XL, Kurths J. *J Appl Mech-T ASME* 2017;84(091004).